Transport and Binding of Insulin-Like Growth Factors to Articular Cartilage

by

Nóra Szász

Submitted to the Department of Electrical Engineering and Computer Science
in partial fulfillment of the requirements for the degrees of

Bachelor of Science

and

Master of Engineering

at the

MASSACHUSETTS INSTITUTE OF TECHNOLOGY

May 1999
[June 1999]

Author .....
Department of Electrical Engineering and Computer Science
May 21, 1999

Certified by .....
Alan J. Grodzinsky
Professor of Electrical, Mechanical, and Bioengineering
Thesis Supervisor

Accepted by .....
Arthur C. Smith
Chairman, Department Committee on Graduate Students

Transport and Binding of Insulin-Like Growth Factors to Articular Cartilage

by

Nóra Szász

Submitted to the Department of Electrical Engineering and Computer Science
on May 21, 1999, in partial fulfillment of the
requirements for the degrees of
Bachelor of Science
and
Master of Engineering

Abstract

Cartilage is capable of withstanding high shear and compressive stress without damage, but its homeostasis is easily disturbed, causing tissue degradation. Reversal of this damage is almost impossible due to the low cell count and perfusion rate of the tissue. It has been shown, however, that certain cytokines are capable of inhibiting and even reversing tissue degradation. For example, insulin-like growth factors are known to stimulate proteoglycan biosynthesis and inhibit matrix degradation.

Currently, two insulin-like growth factors are known: IGF-I and IGF-II. Both of these cytokines were found to stimulate tissue regeneration in vitro, even though in vivo studies have been unsuccessful due to the slow transport of the growth factors to the target cells. It has also been established that growth factors bind to the tissue in much greater amounts than those accounted for by cell receptor binding. The exact binding sites, however, are still unknown.

Research has shown that IGF-II has a higher affinity for binding sites than IGF-I, and can therefore successfully compete with IGF-I. The goal of this study was to describe the kinetics of transport and binding of these growth factors in cartilage. While there have been some previous studies on the transport of IGF-I in bovine and human cartilage, there is little information on transport of IGF-II. The diffusivity of IGF-II was measured to be on the order of $10^{-7}\frac{cm^2}{s}$, and the characteristic lag time was approximately 180 minutes for a $350\mu m$ thick cartilage disk. These parameters characterize the fundamental chemical and mechanical kinetics of IGF transport within the tissue. Future studies will focus on further characteristics of macromolecular transport within cartilage.

Thesis Supervisor: Alan J. Grodzinsky
Title: Professor of Electrical, Mechanical, and Bioengineering

Acknowledgments

This thesis would not have been possible without the help of

- Prof. Alan Grodzinsky, my supervisor, who led me into a new field, and provided advice and enthusiasm throughout my work,
- Eliot Frank, who helped me fix what was broken, and beat the experiments into submission,
- Teresa Morales, who has helped me force the growth factors do their duty,
- Linda Bragman, who helped me fight the eternal bureaucracy,
- The Continuum Electromechanics Group, who made the lab a fun place to be,
- MIT, which believed I could succeed four years ago, and gave me that trust for the next four (five? six?) years,
- Boris Zbarsky, who was at the receiving end of all my frustrations during these past few weeks,
- Prof. Jane Dunphy, who taught me how to write without making my readers cringe,
- Several of my high school teachers — Flórik György, Tóth Attila, and Czirók Ede — who have given me my love for science, and
- My parents, who have given me all that I have.

Thank you.

This research was sponsored in part by NIH Grant AR33236.

Contents

List of Figures

List of Tables

List of Symbols

BSA	Bovine Serum Albumin
CS	Chondroitin-Sulfate
ECF	Extracellular Fluid
ECM	Extracellular Matrix
EDTA	[ethylenedinitrilo]tetraacetic acid
G1, G2, G3	Globular regions of aggrecan's core protein
GAG	Glycosaminoglycan
HA	Hyaluronan
IGF	Insulin-Like Growth Factor
IGF-BP	Insulin-Like Growth Factor Binding Protein
KS	Keratan-Sulfate
MMP	Matrix Metalloproteinase
OA	Osteoarthritis
PBS	Phosphate Buffered Saline
PG	Proteoglycan
PI	Protease Inhibitor
PSA	Penicillin, Streptomycin, and Antibiotics
RA	Retionic Acid
TGF	Transforming Growth Factor
TIMP	Tissue Inhibitor of Metalloproteinases

Chapter 1

Introduction

1.1 Background

Articular cartilage is a highly durable weight-bearing material in the synovial joint. Its durability and resilience to compression are highly dependent on the composition of its extracellular matrix, which is maintained by a small number of cells. Since cartilage is avascular and alymphatic, its perfusion rate is low, and, therefore, the production of the matrix elements is limited by the transport of nutrients, waste, and regulatory solutes within the tissue.

Normally, nutrients can still be supplied to the cells and toxic waste can be removed despite the low perfusion rate, but if the tissue is injured, a higher perfusion rate might be required for tissue regeneration [1, 2]. The anatomy of cartilage suggests that the transport of nutrients, waste, and regulatory solutes should be limited by diffusion. Studies have shown, however, that a coupling between mechanical, electrical, and chemical forces can enhance transport and result in a higher tissue perfusion rate, thus increasing tissue biosynthesis. The stimulation of cartilage tissue by dynamic mechanical loading and the use of variable electric fields have both been used to achieve increased fluid, and hence nutrition, flow.

1.2 Objective

The mechanisms that affect the synthesis of cartilage matrix by chondrocytes are not yet fully understood. It is known that growth factors play an important stimulatory role.

Therefore, it is beneficial to describe the rate at which these stimulatory cytokines reach the cells, and the components to which they bind. The objective of this study has thus been to characterize the binding and transport kinetic properties of insulin-like growth factors (IGFs) within bovine articular cartilage, in order to create a quantitative description of their transport and establish a relationship between IGFs and chondrocyte biosynthesis.

1.3 Overview

The first part of this thesis, Chapters 2–3, establishes the groundwork for the experimental studies. Chapter 2 describes the unusual biological properties of cartilage and introduce the structure and function of insulin-like growth factors. Chapter 3 provides the theoretical background for my calculations and lays down the groundwork for the coupling of electrical, mechanical, and chemical forces within the tissue.

Chapters 4–7 are the experimental section. Chapter 4 introduces the research that inspired this thesis, and discusses the results and implications. Chapter 5 describes the tests that were necessary to validate the experimental system in use, and Chapter 6 presents a preliminary study describing the transport kinetics of iodide within cartilage. These studies provided the basis for the final experimental chapter, Chapter 7, which presents the experiments and results of the IGF-II transport kinetic experiments.

Finally, Chapter 8 finishes with the conclusion, which summarizes the results and suggests what further studies should be done for a more complete description of the transport kinetics and binding of IGF-II.

Chapter 2

Articular Cartilage

Articular cartilage provides cushioning, lubrication, and load distribution over bone surfaces inside joints. Due to its special function, cartilage has to be resilient, but capable of undergoing limited deformation. Although articular cartilage is tough, it is composed of mostly water and has a low cell concentration in adult bovine cartilage. The low cell concentration and avascular anatomy of cartilage make it difficult for cartilage to regenerate after injury; because of this, it is important to study the transport of macromolecules and nutrients inside the tissue to determine ways of facilitating tissue healing after injury.

2.1 Articular Cartilage Anatomy

Articular cartilage covers articulating bone surfaces and provides cushioning, lubrication and load distribution. It is avascular and alymphatic, which makes the transport of nutrients difficult within the tissue. The tissue itself is composed of 70–80% water by weight [3] in which a sparse, $2 \cdot 10^4$–$4 \cdot 10^4 \frac{cells}{mm^3}$, population of cells is embedded [4, 5]. This density of cells is sufficient to maintain the extracellular matrix (ECM) under normal conditions, but it may be too low for proper regeneration of the tissue after injury.

The extracellular matrix is highly charged and provides the extreme strength and durability of the tissue, even though it is mostly composed of water. The most important macromolecules of the ECM are collagen ($> 55\%$ by dry weight) and proteoglycans (PG) ($> 35\%$ by dry weight). The collagen gives the tissue shear and tensile strength, while the highly charged proteoglycans provide the compressive strength of the tissue [5].

The physiological turnover of the ECM relies on the delivery of nutrients and the removal

of waste. Since the tissue contains neither a vascular nor a lymphatic system, the exchange of nutrients and waste is presumed to occur by diffusion and compression induced convection of the extracellular fluid (ECF).

The delivery of large regulatory solutes also plays a key role in homeostasis and biosynthesis. Some of the most important regulatory solutes are the insulin-like growth factors, (IGF)-I and IGF-II. Both IGFs have been found to reduce matrix degradation and stimulate proteoglycan synthesis in vitro [6, 7]. Therefore, the transport kinetics of these solutes play a key role in the regeneration of cartilage tissue after injury.

2.1.1 Chondrocytes and the Chondron

The cartilage cells, or chondrocytes, build and maintain the cartilage. Although they are few in number, they play a very important role in the physiological turnover of the ECM. Chondrocytes generate the extracellular matrix, which is responsible for the extraordinary properties of cartilage. Since cartilage is avascular, nutrition is scarce and transport limited. Thus, chondrocytes are specialized to use anaerobic pathways and prefer them even in aerobic conditions [8].

Another notable property of the chondrocytes is their lack of detectable cell division in healthy adult cartilage. Contrary to most cells in the human body, the majority of chondrocytes live and function for the entire life span of a healthy individual. If cartilage is damaged, the cells start to divide at a very slow rate. This rate is limited by the transport of nutrition and growth factors. Aging can also decrease the chondrocyte count. The cell count in human costal cartilage was found to decrease by 25% by the age of 30. This can partially explain the increased difficulty of cartilage repair in the elderly.

Even though chondrocytes normally do not divide, and, in case of injury, their reproduction rate is low, it has been shown that they are capable of reproducing rapidly under abnormal conditions. For example, if chondrocytes are grown as mono-layer cultures, they are found to undergo rapid proliferation in vitro [9].

Due to its weight-bearing function, cartilage must tolerate peak stresses of $10 - 20MPa$ during stair climbing, for example. A load of this magnitude could easily damage a cell. In adult cartilage, chondrocytes, therefore, create a compression-resistant, fluid-filled pocket, known as chondron, that dampens environmental extremes such as high mechanical stress, osmotic changes and physico-chemical changes [8]. Chondrons are extremely complex and

heterogeneous structures built to cradle the cell. They are composed of type II, VI and IX collagen, several proteoglycan epitopes, and glycoproteins such as fibronectin. They are oriented parallel to the lines of force operating in situ to further reduce stress [8].

Cartilage is far from homogeneous. A variation in cell, collagen, and proteoglycan density can be observed in articular cartilage. The cell density varies inversely with the cartilage thickness, and it is greatest near the surface of the cartilage [4].

2.1.2 Extracellular Matrix

The extracellular matrix (ECM) is composed of more than 55% of collagen by dry weight, and more than 35% of PG by dry weight [5]. Another important but minor constituent of the ECM is hyaluronan (HA). Hyaluronan molecules have long random coil structures, providing the backbone to which chondrocytes attach [8] and the scaffolding for the macromolecules of the ECM.

2.1.3 Collagen

Collagen is the most important structural protein in the human body. It is composed of three left-handed helical polypeptide chains supercoiled into a single right-handed triple-helix. The third residue of each chain is a glycine, and the chains are staggered by one residue relative to one another, hence allowing close packing by turning the glycine residue toward the middle of the helix [10].

Collagen is responsible for the integrity and tensile strength of cartilage due to its abundant cross linkages and stable structure. Cartilage contains several types of collagen, each having a slightly different function. The functions and quantities of the most important types are summarized in Table 2.1 [11, 5, 12].

2.1.4 Proteoglycans

Proteoglycans have a core protein and one or more covalently attached glycosaminoglycan (GAG) chains. The structure of the core protein varies widely from the 20kDa serglycin, to the 200–350kDa core protein of aggrecan [13]. Aggrecan, which is the most abundant PG in cartilage, provides the tissue with an incredible compressive stiffness due to the highly charged GAG chains attached to its core protein. Figure 2-1 shows a schematic diagram of a typical aggrecan [14].

TYPE	QUANTITY	FUNCTION
II	$> 90\%$	tensile strength, stiffness
VI	$< 1\%$	lateral strength, flexibility
IX	$\sim 1\%$	connections between fibrils
X	$< 1\%$	unknown
XI	$\sim 3\%$	fibril formation

Table 2.1: Type, quantity, and function of the most relevant collagen molecules found in adult articular cartilage.

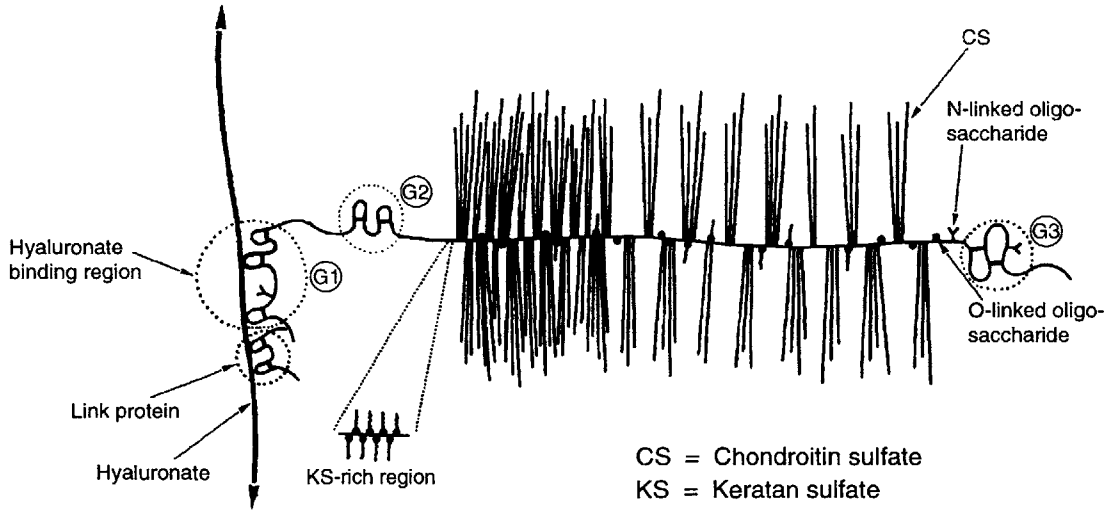

Figure 2-1: Schematic diagram of a typical aggrecan. (Figure has been taken from Heinegard et al.)

The core protein of aggrecan contains three globular regions. The first globular region, G1, is located near the N-terminal, and is used to attach to the binding region of hyaluronate using a link protein. Further down the core protein is the second globular region, G2, and all the way at the C-terminal resides the third globular region, G3. The highly charged GAG rich region is located between G2 and the G3 [5].

Aggrecan contains three major types of glycosaminoglycans: chondroitin-6-sulfate, chondroitin-4-sulfate, and keratan-sulfate (KS). The keratan-sulfate chains are the shortest ($\sim$ 5kDa) consisting of approximately 10 repeating disaccharide units. These chains are located near the G2 region of the core protein. The chondroitin-sulfate (CS) chains dominate the rest of the core protein contributing a significant carbohydrate portion that comprises 95% of the molecular weight of the entire proteoglycan molecule [5].

Chondroitin contains negatively charged carboxylate and sulphate groups, while keratan-sulphate contains negatively charged sulphate groups. The electrostatic interactions of the negative charges provide the compressive strength of cartilage. To achieve this strength, cartilage normally contains $100\frac{mg}{ml}$ GAG, making it one of the most highly charged tissues in the human body [5].

2.2 Regulatory solutes

It has been found that certain regulatory solutes are capable of stimulating the biosynthesis and/or decreasing the degradation of proteoglycans in vitro. Some of the regulatory solutes that have been studied are IGF-I [7], IGF-II [15], tissue inhibitors of metalloproteinases-1 (TIMP-1) [5], and transforming growth factor-β (TGF-β) [7].

Tissue inhibitors of metalloproteinases (TIMPs) are a family of matrix metalloproteinase (MMP) inhibitors. Matrix metalloproteinases are responsible for degrading PG molecules inside cartilage. TIMPs prevent the degradation of PG by inhibiting MMPs. While the concentration of TIMP is slightly greater than that of MMPs inside a healthy tissue ($\sim$ $1.1\frac{\mu g}{ml}$), osteoarthritic cartilage has only about half of this concentration. Thus, the lack of sufficient MMP inhibitors can explain the PG loss observed in diseased cartilage.

Less is known about the function of TGFs and IGFs. In previous studies Morales [7] has shown that TGF-β and insulin-like growth factor-1 can restore proteoglycan metabolism of bovine articular cartilage after depletion by retinoic acid (RA). Her results showed that $10\frac{ng}{ml}$

of TGF-β could restore $74\% \pm 24\%$ of PG synthesis, $10\frac{ng}{ml}$ of IGF-I could restore $69 \pm 18\%$ of PG synthesis, and their combination could restore as much as $95 \pm 17\%$ of PG synthesis in one week. This suggests that TGF-β and IGF-I induces synthesis of proteoglycan aggregates through a coordinated increase in hyaluronan and aggrecan [7, 15], and inhibits matrix degradation induced by retinoic acid (RA) [6]. The fact that the PG loss was not recovered after a week, however, indicates that other factors, such as other cytokines or mechanical forces, might be involved in cartilage regeneration.

2.2.1 Insulin-like Growth Factors

IGF-I and IGF-II are single-chain polypeptides. As the name suggests, they are homologous to both insulin and one another. They all share three disulfide bridges, 45% of their amino acids, and have similar 3-D structures. Due to these similarities, the three peptides exhibit similar functional and binding properties. For example, IGF-I has been shown to bind insulin receptors [16]. The molecular weight of both growth factors are around $7.6kDa$. The molecular radius is approximately 1.2–1.3nm. IGF-I concentration in cartilage is between $1\text{–}50\frac{ng_{IGF}}{g_{tissue}}$. Figure 2-2 shows the stereo view of IGF-I and IGF-II.

It has been shown that the concentration of IGF-I is increased in osteoarthritic synovial fluids. It has also been found that the concentration of IGF-I within normal cartilage is low due to exclusion of large particles by the tissue; however, the concentration of the growth factor in osteoarthritic cartilage can be an order of magnitude higher. Since higher levels of growth factors were found to stimulate ECM regeneration, it is assumed that the increased presence of IGF-I is a defensive measure of the body against the disease [17].

It has also been noticed that IGF-I reversibly binds to cartilage in much greater amounts than would be predicted by cell receptor binding or the partition coefficient calculated from the molecular size. Therefore, Schneiderman et al [15] hypothesized that IGF-I also binds to matrix components. This was supported by their finding that cartilage contained specific, probably cell receptor, and non-specific, probably PG, binding sites. Other research suggests, that what Schneiderman et al. believed to be non-specific ECM binding sites could be attributed to IGF binding proteins (IGF-BP) [18, 19].

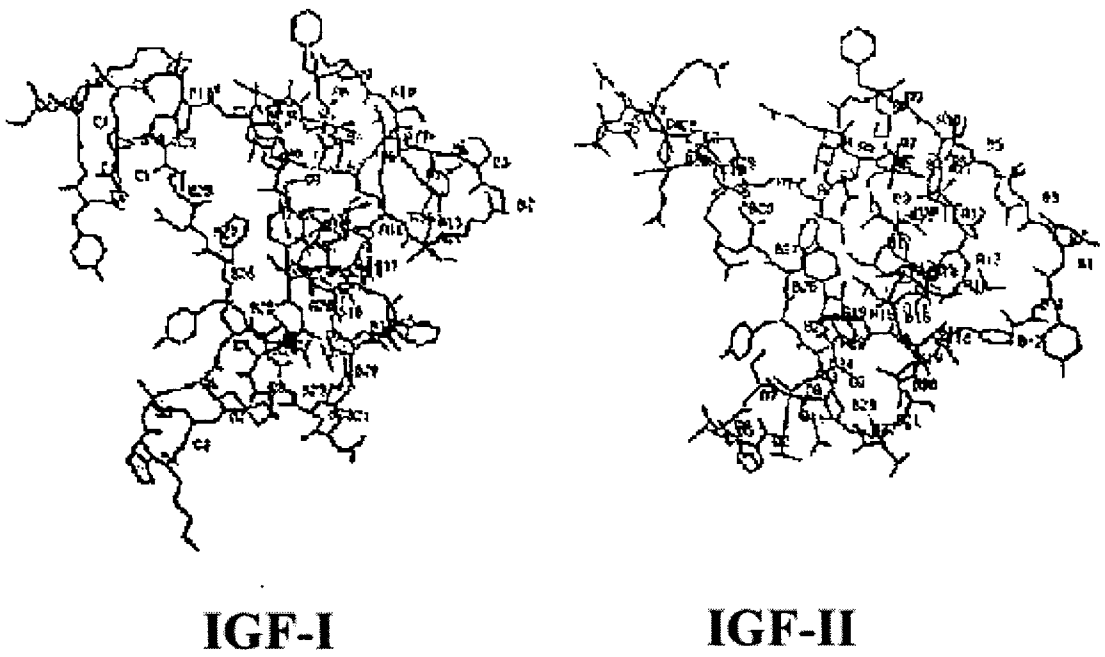

Figure 2-2: Stereo view of IGF-I and IGF-II.

Chapter 3

Transport Kinetics

3.1 Diffusion

Concentration gradients of a solute in a medium disappear over time. This phenomenon is known as diffusion. The goal, is to characterize the diffusion of growth factors in cartilage tissue, to help describe the kinetics of IGF-II, and possibly to use this knowledge to enhance tissue growth and regeneration.

3.1.1 Fick's Laws

The diffusion of particles was first described empirically by Fick in 1855 [20]. *Fick's First Law* describes the relationship between the flux of a chemical species and the concentration gradient of that species [21]:

$$\mathbf{\Gamma}_i = -D\nabla c_i, \tag{3.1}$$

where $\mathbf{\Gamma}_i$ $[\frac{moles}{cm^2 s}]$ denotes the flux of the ith species, D $[\frac{cm^2}{s}]$ is the diffusion coefficient, and ∇c_i $[\frac{moles}{cm^4}]$ is the concentration gradient of the ith species.

Experiments were done in a two-chamber system (Figure 3-1) in which the two chambers have uniform, but distinct, concentrations of a labeled species. The concentration gradient is zero everywhere except in the membrane that separates the two chambers. After an initial lag time, τ_{lag}, a steady-state, linear concentration profile is established in the membrane. In steady-state, Fick's Law can be simplified to *Fick's First Law for Membranes* [21]:

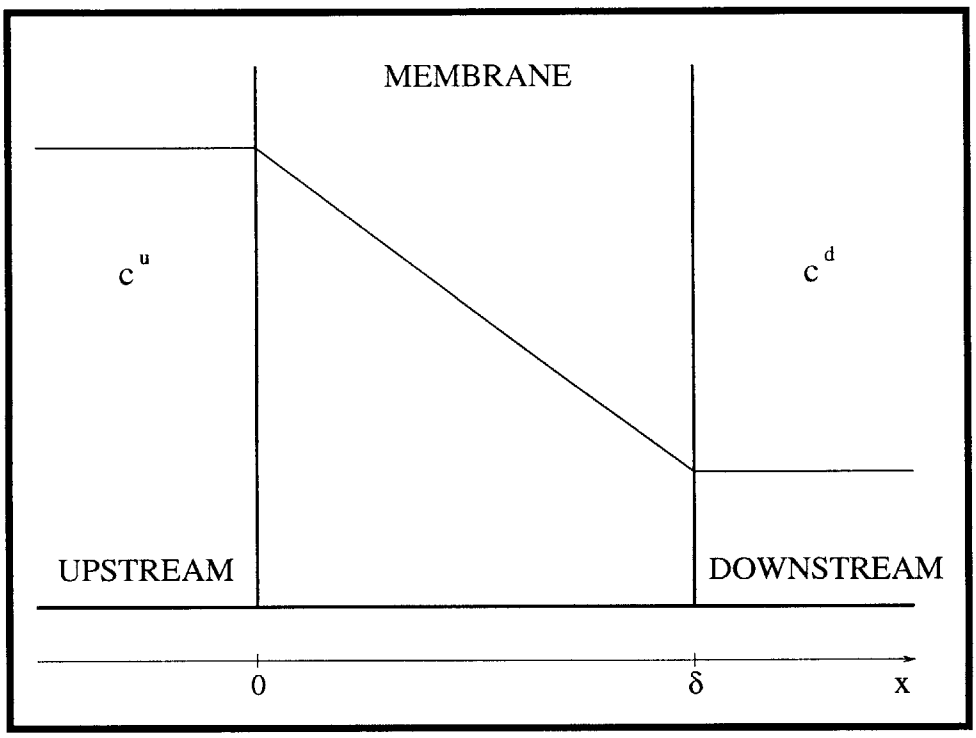

Figure 3-1: Definition of variables involved in deriving relations for steady-state diffusion across a membrane and infinitely large baths on both sides.

$$\Gamma_i = -D\frac{\Delta c_i}{\delta}, \tag{3.2}$$

where δ $[cm]$ is the thickness of the membrane.

Since only the percentage of the total amount of solute that had diffused from the upstream chamber to the downstream chamber could be measured, we used a *normalized flux*, defined as the percentage of the total solute that has diffused across a unit membrane area in a unit of time. We also used *normalized concentration*, which corresponds to the percentage of the total solute in a unit volume of solution. Hence the diffusion coefficient can be found from measurable variables as follows:

$$D = \frac{\delta\ V^d}{\Delta t\ A}\left(\frac{N(t+\Delta t) - N(t)}{\overline{N^u} - \overline{N^d}}\right), \tag{3.3}$$

where V^d $[m^3]$ is the downstream bath volume, Δt $[min]$ is the time between measurements, A $[m^2]$ is the area of the membrane, $N(t)$ [%] is the measured solute percentage downstream at time t, and $\overline{N^u}$ and $\overline{N^d}$ [%] are the average percentages of solute in the upstream and

downstream chambers respectively.

If we consider a fixed control volume of some solution, the solute that enters through the boundaries of this control volume must increase the concentration inside appropriately. This relationship is described quantitatively by the *continuity equation*, also known as *Fick's Second Law* [21]:

$$\frac{\partial c}{\partial t} = D\nabla^2 c. \tag{3.4}$$

Fick's First and Second Laws provide enough information to describe the purely diffusive transport kinetics of any solute in a medium.

3.1.2 Stokes-Einstein Model

It is possible to give a theoretical estimate of the diffusion coefficient in bulk media given the radius of the solute and the viscosity of the medium. The model used to describe this relationship was presented by Einstein in 1908 [22], and is known as the Stokes-Einstein model. The Stokes-Einstein model capitalizes on the fact that in steady-state the velocity of an average particle is constant; hence, the average of the forces acting on a particle must cancel. This force balance equation is:

$$\kappa T \frac{\partial(\ln c_i)}{\partial x} + f v_{ix} = 0, \tag{3.5}$$

where $\kappa = 1.38 \cdot 10^{-23} \frac{J}{K}$ is Boltzman's constant, T $[K]$ is the absolute temperature, f $[\frac{sN}{m}]$ is the drag coefficient, and v_{ix} $[\frac{m}{s}]$ is the x-component of the particle's velocity with respect to the medium. In this equation, the first term is the force acting on a single particle due to a chemical potential gradient and the second term is due to fluid drag [23].

Generalizing Equation 3.5 to multiple particles in a control volume and using Stokes's Law [24] to find the value of f, we see that:

$$D = \frac{\kappa T}{f} = \frac{\kappa T}{6\pi\mu r_i}, \tag{3.6}$$

where μ $[s\,Pa]$ is the viscosity of the solution and r_i $[m]$ is the solute radius. This equation is known as the *Stokes-Einstein Equation.*

The solutes used in the experiments were iodide and IGF-II; thus a theoretical estimate

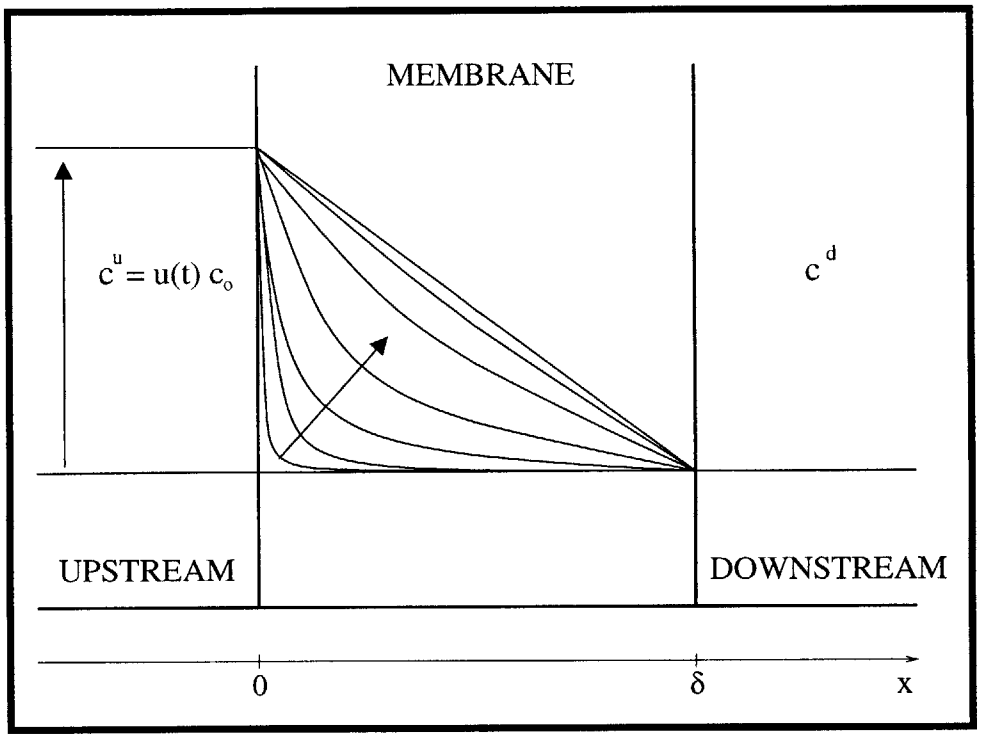

Figure 3-2: Evolution of the concentration profile in a membrane due to a step increase in the concentration on the left side of the membrane.

of the diffusion coefficient of both solutes could be calculated based on their radii using the Stokes-Einstein Equation. The theoretical values of the diffusion coefficients at $9°C$ in water are:

$$D_I = 9.56 \cdot 10^{-7} \frac{cm^2}{s} \quad \text{and} \quad D_{IGF} = 1.65 \cdot 10^{-7} \frac{cm^2}{s}. \tag{3.7}$$

The actual value of the diffusion coefficient in cartilage is predicted to be much lower than the bulk value, since the movement of the solute is hindered by steric and electrostatic forces.

3.1.3 Non-Steady-State Kinetics

Steady state is not established instantaneously. It is easy to see that if the concentrations of the baths are equal for $t < 0$, and a step in the left bath concentration is introduced at $t = 0$, the concentration profile in the membrane will not be linear. Figure 3-2 shows the evolution of the concentration profile within the membrane as modeled using Fourier series approximations. The longest time constant of the Fourier series is the so-called *steady-state*

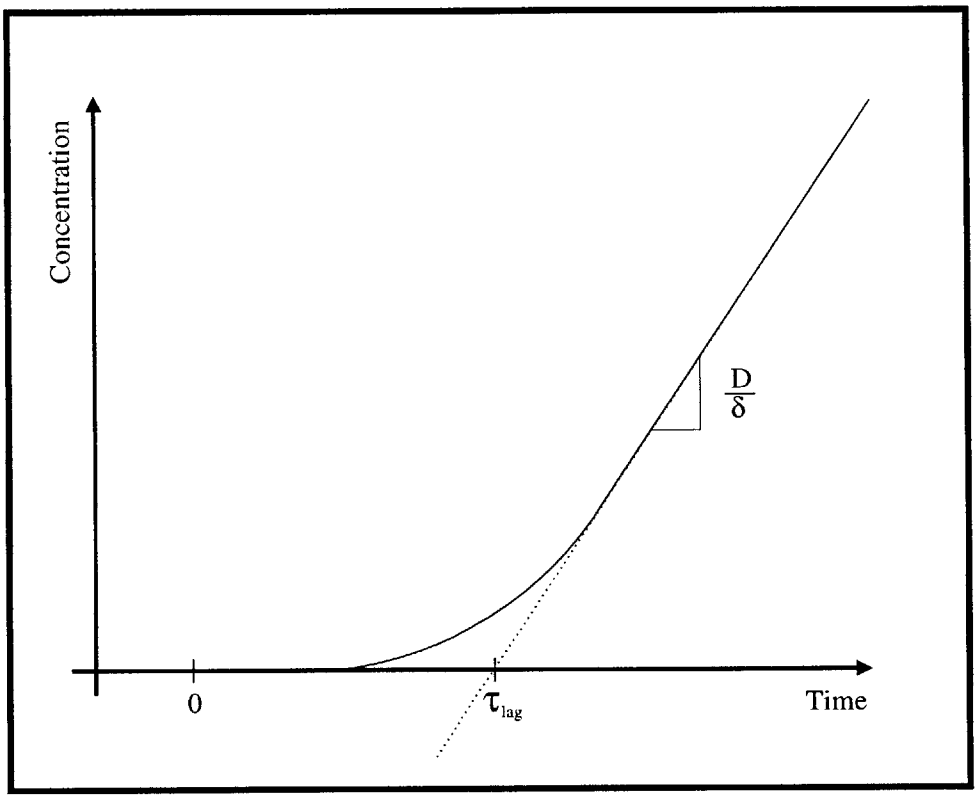

Figure 3-3: The theoretical quantity of solute that has diffused across the membrane by time t.

time constant, τ_{SS}, which is a generally used characteristic time constant:

$$\tau_{SS} = \frac{\delta^2}{\pi^2 D}. \tag{3.8}$$

For us, however, a more important time constant is the lag time, τ_{lag}, which is the time lag from the onset of the step function until the linear steady-state curve intersects the original constant concentration profile (Figure 3-3). This value can be found from the general flux equation:

$$\tau_{lag} = \frac{\delta^2}{6D}. \tag{3.9}$$

3.1.4 The Effect of Binding

Growth factors signal cells by binding to the cells and possibly to the extracellular matrix. The binding of a growth factor can be measured by analyzing the perturbed transport kinetics of the solute. If the only driving force on the solute is the concentration gradient,

a mathematical model can be derived that will allow us to calculate the percentage of the growth factor that has bound to the tissue. This model also enables the analysis of competitiveness between the various growth factors and the time scales of binding and competition between the species.

The binding of a growth factor to the cartilage can be modeled as a second-order reversible reaction:

$$S + E \underset{k_d}{\overset{k_a}{\rightleftharpoons}} ES, \tag{3.10}$$

where S represents the unbound solute (growth factor), E represents free binding sites, and ES stands for solutes bound to a binding site.

In most cases, we can assume that the concentration of binding sites is a constant, c_{ET}, and that steady-state is reached instantaneously; hence

$$K = \frac{k_d}{k_a} = \frac{c_S\, c_E}{c_{ES}} \quad \text{and} \quad c_{ET} = c_{ES} + c_E, \tag{3.11}$$

where K $[\frac{moles}{cm^3}]$ is the *dissociation constant.*

We can use Fick's Second Law to incorporate binding into the diffusion equation as follows:

$$\frac{\partial}{\partial t}(c_S + c_{ES}) = D\frac{\partial^2 c_S}{\partial x^2}. \tag{3.12}$$

Combining Fick's Second Law with the chemical binding term, we can find the new expression for diffusion:

$$\frac{\partial c_s}{\partial t} = \frac{D}{1 + \frac{c_{ET}K}{(K+c_S)^2}}\frac{\partial^2 c_S}{\partial x^2} = D_{eff}\frac{\partial^2 c_S}{\partial x^2}. \tag{3.13}$$

Note that the new effective diffusion coefficient depends on the solute concentration and is less then the actual diffusion coefficient. Binding of the solute to the tissue will therefore slow transport across the tissue in the beginning, increasing the length of the lag time.

3.2 Migration

The application of an electric field to certain media creates a current. If this current is due to the motion of ions, this phenomenon is called migration. The current induced by an electric field depends on the strength and direction of the electric field and the properties of the medium. For this study we assume that our medium, cartilage, is a homogeneous ohmic conducting material, and that the system is electroquasistatic. A material is called ohmic if it follows Ohm's Law (Section 3.2.1). A system is electroquasistatic if the time varying magnetic field is negligible, and thus Faraday's induction law simplifies to

$$\nabla \times \mathbf{E}(\mathbf{r}, t) = -\frac{\partial \mathbf{B}(\mathbf{r}, t)}{\partial t} \approx 0. \tag{3.14}$$

This simplification allows us to introduce a new variable, Φ $[V]$, known as the electrical potential, defined as

$$\mathbf{E} = -\nabla\Phi. \tag{3.15}$$

3.2.1 Ohm's Law

A potential gradient will exert a force on charged particles, creating currents in conductors. In ohmic media, the relationship between the strength of the electric field and the induced current is linear and the constant coefficient is known as the conductivity of the medium. Ohm's Law is hence

$$\mathbf{J} = -\sigma_e \nabla\Phi, \tag{3.16}$$

where $\mathbf{J}$ is the current density $[\frac{A}{cm^2}]$, σ_e is the conductivity of the material, and $\nabla\Phi$ is the potential gradient $[\frac{V}{m}]$.

The movement of ions through a medium due to an applied electric field is known as *electrophoresis*. Electrophoresis can be used to enhance the transport of ions to their destination. In some of the experiments we tested the enhanced transport of iodide and IGF-II across cartilage tissue.

The conductance of a solution is related to the ionic concentration of the solutes. This

relationship can be expressed as:

$$\sigma = \sum_i |z_i| F u_i c_i, \tag{3.17}$$

where i denotes a specific charged species, z_i is the valence of the species, F is Faraday's constant ($F = 96,500 \frac{C}{moles}$), u_i is the mobility of the ith species, and c_i is the concentration of the ith species.

In the calculations it was assumed that cartilage is an ohmic conductor under the experimental conditions.

3.3 Convection

Pressure gradients can induce fluid flow in permeable materials. This fluid flow in a medium is called convection.

3.3.1 Darcy's Law

Convection induced by a pressure gradient can be described by a linear equation in most materials, similarly to diffusion and migration. This equation is known as Darcy's Law and the constant coefficient is the Darcy permeability, κ $[\frac{m^2}{sPa}]$:

$$\mathbf{U} = -\kappa \nabla P, \tag{3.18}$$

where $\mathbf{U}$ is the velocity (i.e. volume flux) of the solvent $[\frac{m}{s}]$, and ∇P is the pressure gradient in the solvent $[\frac{Pa}{m}]$.

In the calculations it was assumed that cartilage obeys Darcy's law under the experimental conditions.

3.4 Coupled Transport Equations

In the previous section we introduced Fick's Law (Eq. 3.1), Ohm's Law (Eq. 3.16), and Darcy's Law (Eq. 3.18). Each one of these laws relates the gradient of an energy source to the movement of either solutes or the fluid. These relationships become more complex, however, if we consider the coupling between them.

3.4.1 The Transport Equations

A potential gradient will induce a current, hence the motion of ions in a solution. The motion of the ions in turn can set the fluid into motion, giving rise to a net fluid flow. Furthermore, the motion of ions constitutes a flux. Hence a potential gradient can create current, fluid flow, and flux.

Similarly, a coupling between chemical and mechanical forces also exists. Both a chemical gradient and a pressure gradient are capable of inducing currents, fluid flow and solvent flux. This relationship can thus be given using phenomenological equations of non-equilibrium thermodynamics [25]:

$$\begin{bmatrix} \mathbf{J} \\ \mathbf{\Gamma_i} \\ \mathbf{U} \end{bmatrix} = \begin{bmatrix} -k_{11} & k_{12} & k_{13} \\ k_{21} & -k_{22} & k_{23} \\ k_{31} & k_{32} & -k_{33} \end{bmatrix} \begin{bmatrix} \nabla\Phi \\ \nabla c_i \\ \nabla P \end{bmatrix}, \tag{3.19}$$

where the k_{ij} are the constant coupling coefficients with appropriate dimensions. Darcy's, Ohm's, and Fick's laws (Equations 3.18, 3.16, and 3.1) are all special cases of Equation 3.19.

The coupling coefficient matrix has some important properties. As the signs indicate, the diagonal elements of the coupling coefficient matrix are all negative. Since the diagonal elements correspond to Darcy's, Ohm's, and Fick's laws, it can be seen that the sign is there to account for "motion" down the "potential" gradients. The second interesting property of the matrix is its symmetric nature. The symmetry exists because from the standpoint of nature it is irrelevant whether a potential drop creates an ionic flow, hence a fluid flow and thus an "effective pressure" or whether a pressure drop creates a creates fluid flow, hence ionic flow, thus an "effective potential." Therefore the coupling coefficient matrix is symmetric, with negative diagonal elements.

Using the above it is possible to calculate the kinetics of solute and solution movement in cartilage. The constant coefficients, however, depend on the composition [26], experimental conditions (pH, ionic strength, etc.), and the orientation of the tissue [27]. In order to be able to quantify experiments carried out on cartilage and find the coupling coefficients, all of the above conditions must be controlled.

The constitutive law given in Equation 3.19 combines electrical, chemical, and mechan-

ical effects, and is thus rarely used in calculations due to its complexity. The single matrix equation combines 3 vector equations, each consisting of 3 components; thus it consists of 9 equations, 9 unknown constants, and 18 variables. To reduce this complexity, the effects of electrical, chemical, and mechanical forces are usually either studied separately, resulting in Ohm's, Fick's and Darcy's laws respectively, or pairwise.

Chapter 4

Previous Work

This section discusses the relevant previous work that shows the stimulation of cartilage biosynthesis in response to enhanced transport due to dynamic electrical and mechanical loading. Furthermore, previous equilibration and transport kinetic studies involving IGF-I and IGF-II in adult bovine cartilage will also be described.

4.1 Stimulation of Biosynthesis by Increased Perfusion Rate

Increased perfusion rate has been shown to stimulate biosynthesis. This has been done by increasing tissue perfusion using dynamic mechanical loading [28, 29] or changing electrical field [30, 31, 26, 32]. The biosynthesis was monitored in most cases by ^{3}H-proline uptake by amino acid and protein synthesis and ^{35}S-sulfate incorporation for GAG synthesis.

It has been found that, at certain frequencies and amplitudes, dynamic mechanical loading of cartilage can cause an increase or inhibition of biosynthesis [28, 29]. The optimal frequency and amplitude for the synthesis of both proteins and GAG chains correspond well to the frequencies and amplitudes at which maximal fluid flow is achieved, but still no cell damage occurs due to the high stresses caused by the loading. The same type of stimulation was found when changing electrical fields were used [31, 32].

4.2 IGF-I and IGF-II Competition for Binding Sites

IGF-I and IGF-II have similar size and structure; hence it can be presumed that they might exhibit similar binding characteristics as well. A simple way to test whether the two growth

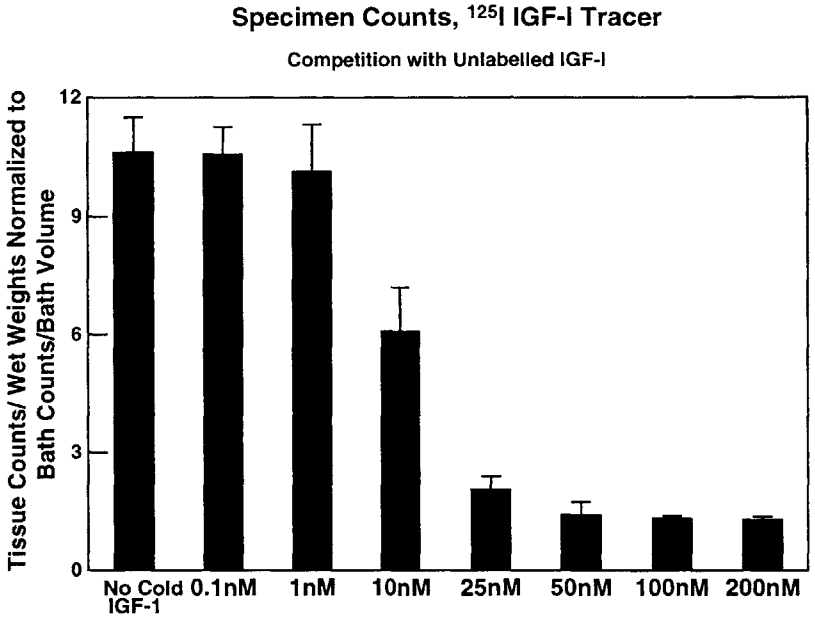

Figure 4-1: Bhakta et al.'s equilibration study showing the competition between labeled and unlabeled IGF-I.

factors exhibit the same binding characteristics is by looking at the competition between IGF-I and IGF-II for binding sites. Experiments characterizing competitive binding of IGF-I and IGF-II have been carried out by Bhakta et al. [19]

For the experiment, $3mm$ diameter and $400\mu m$ thick adult bovine cartilage disks from the femoropatellar groove of 18–24 month steers were used. After an 18–20 hour equilibration period in PBS and protease inhibitors (PI) at $4°C$, the disks were placed in PBS, 0.1% BSA, PI, ^{125}I-IGF-I or ^{125}I-IGF-II and graded levels of unlabeled IGF-I or IGF-II. Following a 48 hour incubation period at $4°C$, the disks were briefly rinsed in $1ml$ PBS enhanced with 0.1% BSA, their activity was counted, and their weight was measured. Figures 4-1, 4-2, and 4-3 show the normalized activity level of the cartilage disks.

The first equilibration experiment tested for competition for binding sites between labeled and unlabeled IGF-I. As Figure 4-1 shows, competition for binding sites does not occur at low growth factor concentrations, but around 10nM, the unlabeled IGF-I starts replacing the radioactive IGF-I indicating a reversible binding and saturation of the binding sites.

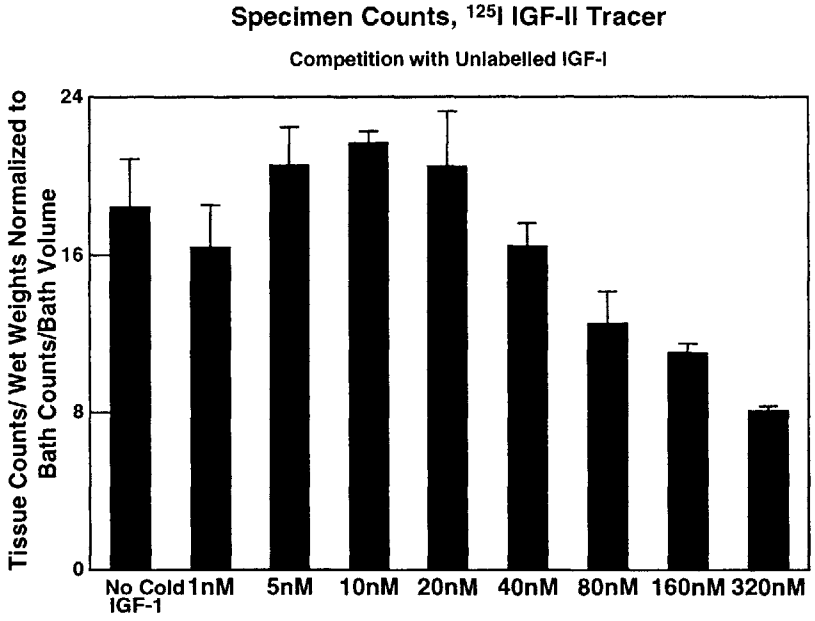

Figure 4-2: Bhakta et al.'s equilibration study showing the competition between unlabeled IGF-I and labeled IGF-II.

Figure 4-2 shows the radioactive ^{125}I-IGF-II content of cartilage specimens after the addition of various amounts of unlabeled IGF-I. It can be seen that the activity of the samples starts decreasing when the concentration of unlabeled IGF-I becomes greater than 40nM. This decrease in the activity is due to the competition between IGF-I and IGF-II for binding sites.

A similar decrease in activity occurs when unlabeled IGF-II competes with labeled IGF-II as shown in Figure 4-3. The concentration of the growth factor at which competition occurs is much lower, however, showing a decrease at a concentration of only 5nM.

From these equilibration studies Bhakta et al. [19] found that the binding of the IGF-I to cartilage is well described by Langmuir a isotherm. Hence, the binding of IGF-I to cartilage is specific. Using Western ligand blotting, they also detected the presence of IGF-BP-6. It has been previously shown that IGF-BP-6 has a higher affinity for IGF-II than for IGF-I. This finding correlates well with the observation that IGF-II competes well with IGF-I, but much higher concentrations of IGF-I are required to compete with IGF-II.

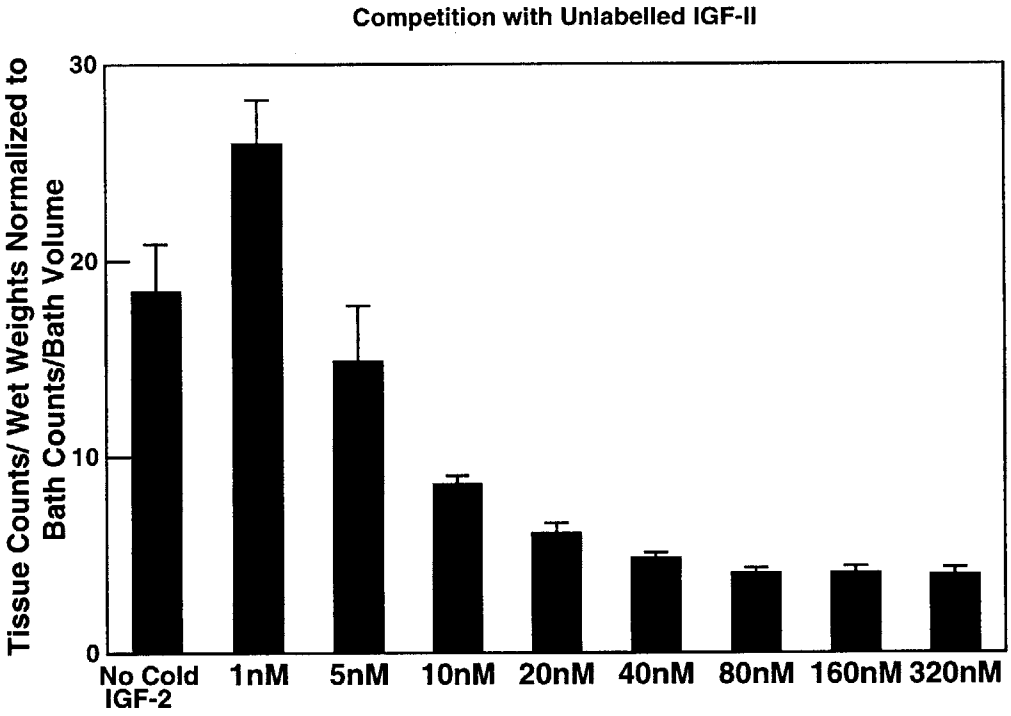

Figure 4-3: Bhakta et al.'s equilibration study showing the competition for binding sites between labeled and unlabeled IGF-II.

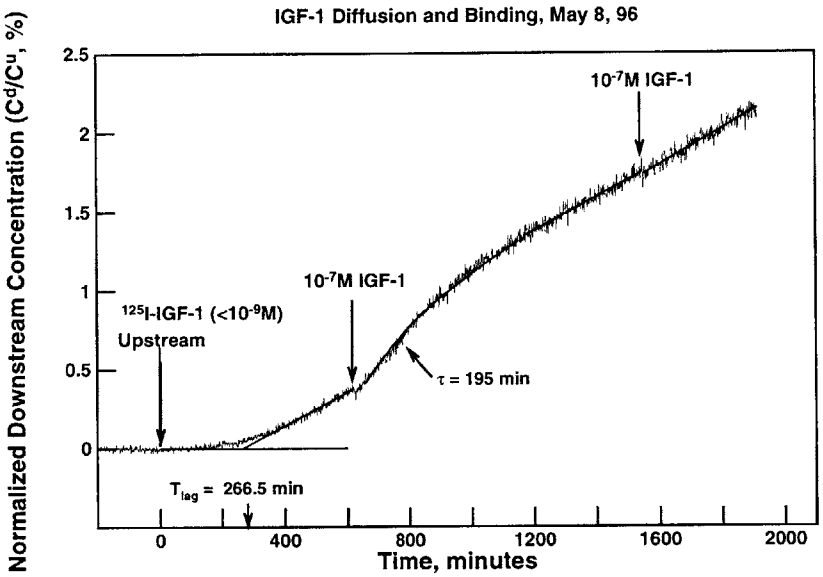

Figure 4-4: Garcia et al.'s transport kinetic study showing the downstream radioactivity of labeled IGF-I.

4.3 IGF-I Transport Kinetic Studies

Garcia et al. [33] studied the transport of IGF-I across bovine cartilage. Two chambers were separated by three $9mm$ diameter plane-parallel disks taken from the femoropatellar groove of adult bovine cartilage. The chambers were filled with PBS, PI, and 0.1% BSA. After a 200 minute equilibration period, radiolabeled IGF-I was added to the upstream chamber, and the downstream activity was monitored by circulating the downstream solution through a gammacounter. After steady-state had been established for several hours, unlabeled IGF-I was added to both chambers. The graph of the downstream counts versus time is presented in Figure 4-4.

The time lag of the labeled IGF-I was measured to be 266 minutes. The lag time calculated from the free IGF-I diffusivity would have been 11 minutes, hence we can see that a considerable amount of binding is present. The diffusion coefficient was also calculated from the steady-state diffusion coefficient, which gave $D = 4 \cdot 10^{-7} \frac{cm^2}{s}$. The addition of unlabeled IGF-I caused a competition between the labeled and unlabeled growth factors for the binding sites; therefore, a transient increase in labeled IGF-I was observed as unlabeled

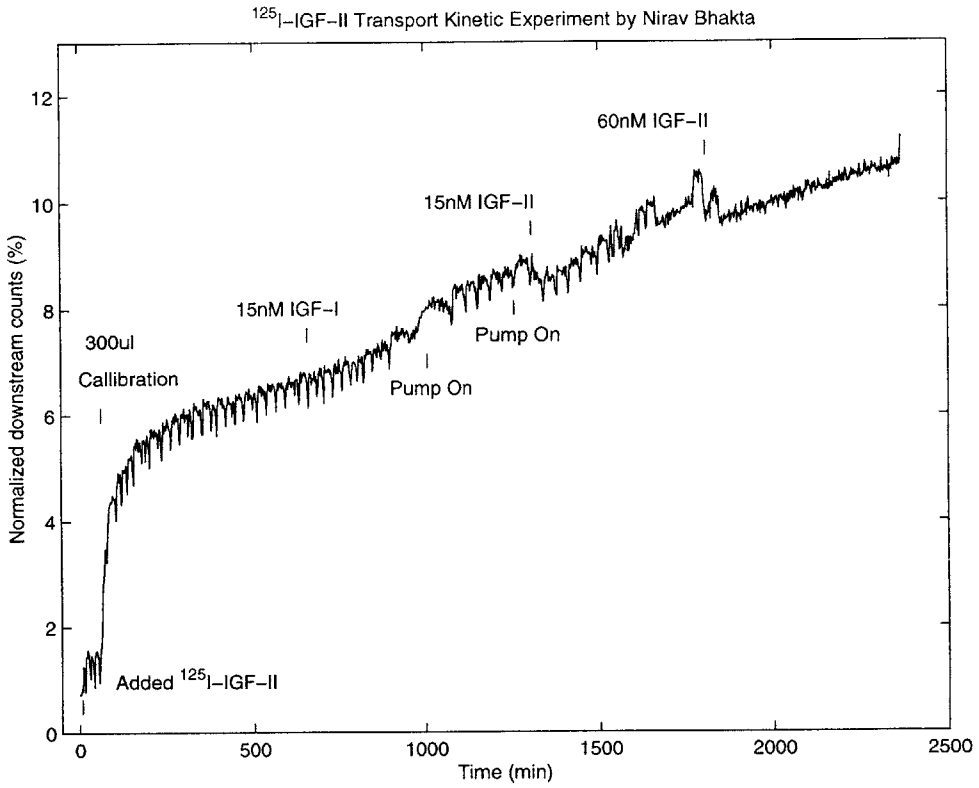

Figure 4-5: Bhakta's IGF-II transport kinetic study showing the downstream count of labeled IGF-II.

IGF-I replaced the labeled IGF-I inside the tissue.

4.4 IGF-II Transport Kinetic Studies

Bhakta [34] also carried out some studies to characterize the transport kinetics of IGF-II by running an experiment similar to the one seen in the IGF-I transport kinetic study (Section 4.3). The goal of these experiments was to establish a steady-state flux of labeled IGF-II across cartilage tissue and to measure the characteristic lag time and diffusion coefficient of the growth factor. Another important feature that Bhakta tried to characterize was the transient kinetics of competition for binding sites between unlabeled IGF-I and labeled IGF-II, and between unlabeled and labeled IGF-II. Figure 4-5 shows the downstream count versus time.

Unfortunately, the pump for the cooling system failed multiple times. It is therefore possible that the integrity of the tissue was compromised during the course of the experiment. However, the steady-state flux of labeled IGF-II was $3.73 \cdot 10^{-5} \frac{\%}{cm^2 s}$ at 500 minutes

into the experiment and $4.32 \cdot 10^{-5} \frac{\%}{cm^2 s}$ at 2000 minutes into the experiment. Since the difference between the steady-state fluxes is small, it is safe to assume that the tissue did not degrade significantly even though the cooling system was not fully operational.

At 650 minutes, 15nM cold IGF-I was added to both chambers. This change did not seem to have any affect on the transport kinetics of labeled IGF-II. This suggests that no competition between IGF-I and IGF-II for binding sites exists at the given concentration levels. This is in agreement with the equilibration studies done earlier by Bhakta et al. [19], in which he determined that competition occurs only for IGF-I concentrations greater than 40nM.

The "bumps" in the curve were probably caused by the recurring difficulties with the cooling apparatus and make the middle section of the data unusable. Hence it is impossible to make a quantitative analysis of the competition for binding sites between the different growth factors.

The data further suggest a possible decrease in the downstream radioactivity after the addition of 15nM IGF-II and 60nM IGF-II. At that point it was yet unknown what might have caused labeled IGF-II to diffuse backwards from the downstream bath to the upstream bath. It was later discovered that this error is probably due to an error in the protocol and should not occur under ideal conditions (Section 7.1.3).

Chapter 5

Experimental Controls

5.1 Testing Binding to the Radiomatic

Binding to the detector of the radiomatic was a serious concern. To test how much radioactive IGF is capable of binding to the detector, a 10% dilution of an upstream sample (after an experimental run) was run through the detector. The dilution was carried out using diH_2O, and the circulation of the diluted sample began at 316 minutes (Figure 5.1).

As was expected, a significant jump was observed in the measured activity to $1650cpm$; however, the activity continued to increase for over 16 hours to a maximum of approximately $2600cpm$ at 1350 minutes. Since our sample contained only 0.01% BSA and $15mM$ NaCl, more BSA and NaCl was added to the solution to create a 0.1% BSA and $150mM$ NaCl solution at 1350 minutes. The effects were dramatic. The radiation dropped by half in about 10 hours, and finally settled around $1000cpm$. Further addition of BSA and NaCl did not reduce binding significantly.

This short control experiment demonstrated the relevance of BSA and high salt concentrations in the system. It also demonstrated that attention must be payed to the experimental setup in order to ensure that I am truly measuring transport through and binding to the sample tissue and not experimental error due to non-specific binding.

5.2 Resistance of the Baths

The conductivity of the baths can be calculated from the ionic concentrations using equation 3.17:

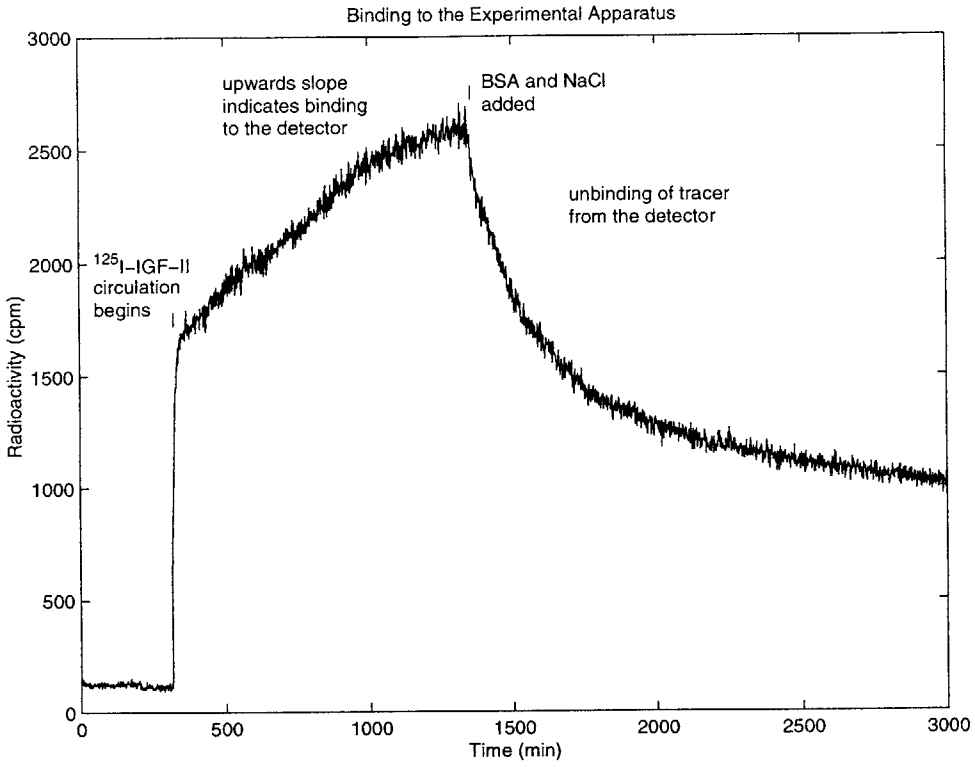

Figure 5-1: Effects of BSA and NaCl concentration on binding to the experimental apparatus.

$$\sigma = \sum_i |z_i| F c_i u_i \approx F c_{Cl} u_{Cl} + F c_{Na} u_{Na}, \tag{5.1}$$

hence

$$\sigma = 96,500 \frac{C}{moles} 0.3 \frac{moles}{L} (5.19 + 7.91) \cdot 10^{-4} \frac{cm^2}{\Omega C} = 3.792 \cdot 10^{-2} \frac{S}{cm}. \tag{5.2}$$

The values used for the electrical mobilities of the ions are the bulk mobilities [35]. The actual mobilities in $150nM$ NaCl solution are about 10% lower.

Using the conductivity of the solution, it is possible to calculate the resistance of the bath:

$$R = \frac{\delta}{A} \cdot \frac{1}{\delta} \approx 25\Omega. \tag{5.3}$$

Since the total resistance measured across the electrodes was 800Ω, the 25Ω resistance of the baths contributes only a 5% error to the calculations; thus, we did not correct for it.

Chapter 6

Free Iodide Transport

The diffusion of $^{125}I^-$ was studied across a cartilage disk in the absence and presence of a current density (J) as a control for later experiments. The purpose of the experiment was to establish the diffusion parameters of $^{125}I^-$. This was necessary to test the validity of the calculations for ^{125}I-IGF-II transport, since small fragments containing $^{125}I^-$ label could dissociate from the growth factor.

6.1 Methods

Cartilage from an 18–24 month old steer's intact joint was used in our experiments. The joints were kept fresh at $4°C$ for at most 4 days. The connective tissue was carefully removed to expose the femoropatellar groove, from which multiple $9mm$ wide cores were obtained using a drill. We removed the topmost layer of cartilage and we cut 1–2 approximately $400\mu m$ thick slices of cartilage disks using a microtome. The cartilage was kept moist during these operations and later stored it in PSA and EDTA supplemented PBS at $4°C$ up to 24 hours before using it in the experiments.

A two chamber setup was used to measure the diffusion of $^{125}I^-$ across a cartilage disk (Figure 6-1). The upstream chamber was separated from the downstream chamber by a single cartilage disk of $3mm$ radius and $370\mu m$ thickness. The chambers were under constant cooling ($12°C$) and stirring to moderate the degradation of the tissue, to reduce the thickness of the stagnant layer near the cartilage disks, and to create a uniform bath concentration. A fixed current or potential drop across the chambers could be established using salt bridge electrodes for the electrochemical coupling experiments. On the downstream

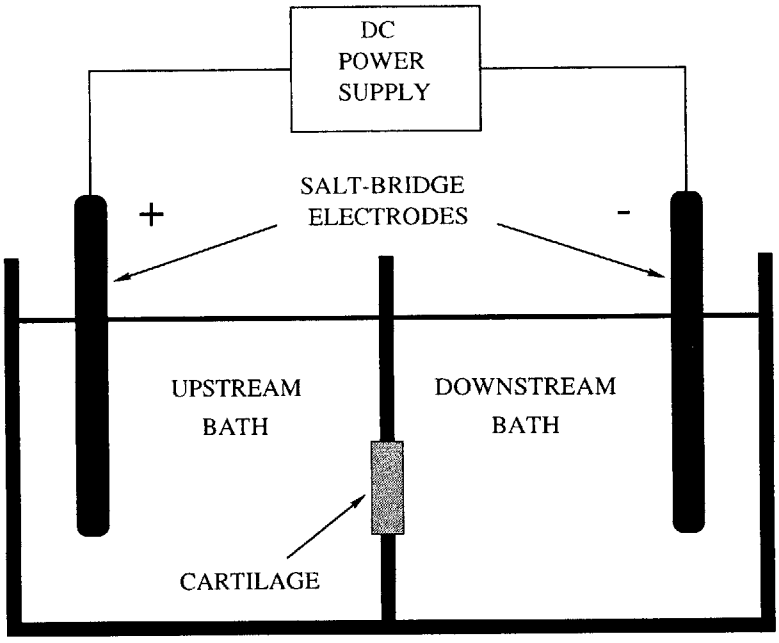

Figure 6-1: Experimental setup for transport measurements.

side, a circulating connection with a gammacounter was created to enable the real-time measurement of $^{125}I^-$ flux across the cartilage disk.

6.2 Results

The downstream radioactivity is graphed versus time in Figure 6-2. The radioactive $^{125}I^-$ was added to the upstream bath at 60 minutes. At 121 minutes the experiment was calibrated by taking 0.4% of the upstream bath volume and adding it to the downstream bath. This allowed the calculation of the percentage of $^{125}I^-$ that had diffused through the cartilage disk into the downstream bath over time, and thus it allowed the normalization of the y-axis with respect to the upstream activity. In steady-state, after calibration, the slope of the downstream radioactivity was $0.29\frac{\%}{hour}$, which corresponds to a steady-state flux of $1.025\frac{\%}{hour\ cm^2}$.

At 192 minutes, $+35.4\frac{mA}{cm^2}$ current density was applied across the chambers for 30 minutes, which gave rise to a potential drop of $8V$ across the chambers. As Figure 6-2 indicates, the radioactivity on the downstream side seems to have remained constant for this period of time, which implies a halt in the movement of $^{125}I^-$ across the cartilage disk. The duration of the applied current, however, was too short to give an accurate measure of the slope.

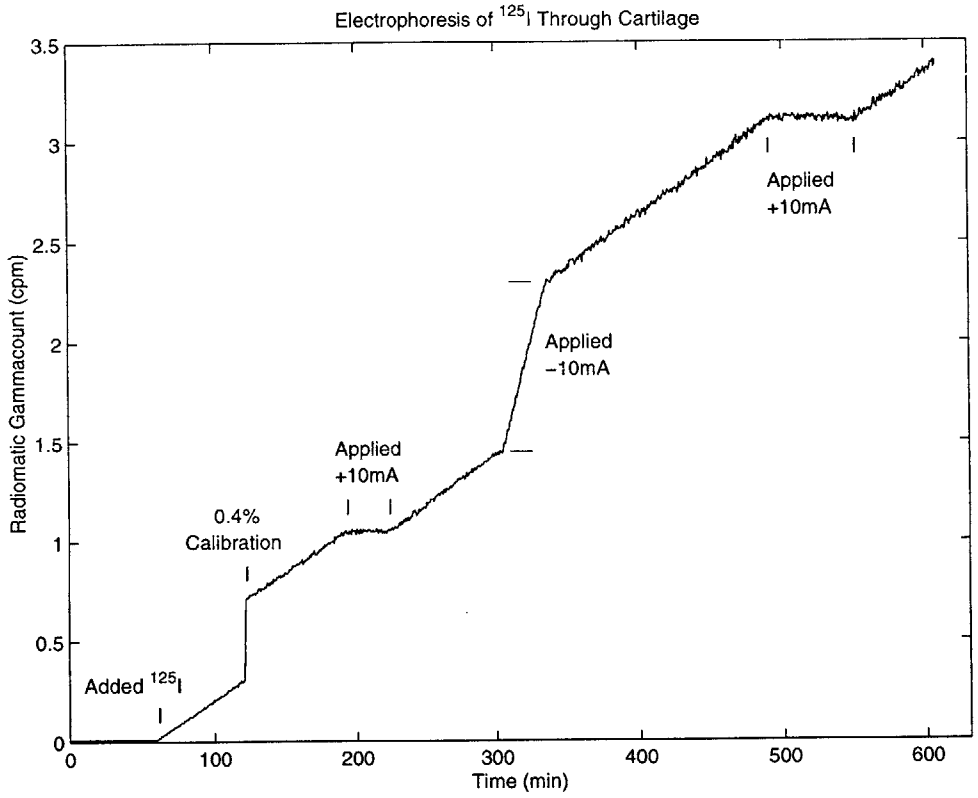

Figure 6-2: Downstream radioactivity for $^{125}I^-$ transport experiment across articular cartilage during electrophoresis.

At 305 minutes, $-35.4\frac{mA}{cm^2}$ was applied for 30 minutes, giving rise to $-8V$ across the chambers. The increase in the slope of the downstream radioactivity from $0.29\frac{\%}{hour}$ to $1.74\frac{\%}{hour}$ is a clear indication of a six fold increase in the $^{125}I^-$ flux from $1.025\frac{\%}{hour\ cm^2}$ to $6.148\frac{\%}{hour\ cm^2}$ due to electrophoresis.

Finally, at 489 minutes, $+10mA$ was applied for another 60 minutes to establish a more accurate measure of the altered slope. The slope for $+10mA$, however, remained approximately $0\frac{\%}{hour}$.

The resistance of the cartilage disk remained 800Ω for all electrochemical experiments. This was measured by taking the ratio of the potential drop and the current across the chambers.

6.3 Discussion

Using the data found in the experiment we can calculate the effective diffusion coefficient of $^{125}I^-$ and the electrical conductance of the cartilage if we assume that the pressure difference between the two chambers is negligible. The coupling between the current density and the solute flux due to a potential and a chemical gradient can be described using the following equation from section 3.4:

$$\begin{bmatrix} \mathbf{J} \\ \mathbf{\Gamma} \end{bmatrix} = \frac{1}{\delta} \begin{bmatrix} -k_{11} & k_{12} \\ k_{21} & -k_{22} \end{bmatrix} \begin{bmatrix} \Delta\Phi \\ \Delta c \end{bmatrix}. \tag{6.1}$$

This equation is equivalent to Equation 3.19 evaluated at $\Delta P = 0$. J $(\frac{mA}{cm^2})$ is the current density across the sample tissue, Γ $(\frac{\%}{min\ cm^2})$ is the normalized flux of iodide across the membrane, $\Delta\Phi$ (V) is the potential drop across the baths, Δc $(\frac{\%}{cm^3})$ is the normalized concentration difference of $^{125}I^-$ between the baths, and the constants k_{ij} are the coupling coefficients.

The values of J, $\Delta\Phi$, Δc, and Γ are known from the experiments, hence we can easily find the value of each coupling coefficient, k_{ij}. Once the values of the coupling coefficients are known, we can use Fick's Law (Eq. 3.1), which applies in the special limiting case when $\Delta\Phi = 0$, to relate the value of k_{22} to the diffusion coefficient, D.

	Current Density, J	Normalized Flux, Γ	Potential Drop, $\Delta\Phi$	Concentration Drop, Δc
I	$0\frac{mA}{cm^2}$	$1.025\frac{\%}{hr\ cm^2}$	—	$-2\frac{\%}{cm^3}$
II	$35.4\frac{mA}{cm^2}$	$0\frac{\%}{hr\ cm^2}$	$-8V$	$-1.94\frac{\%}{cm^3}$
III	$-35.4\frac{mA}{cm^2}$	$6.148\frac{\%}{hr\ cm^2}$	$8V$	$-1.96\frac{\%}{cm^3}$

Table 6.1: Experimental results of labeled iodide transport due to concentration and potential gradients.

$$\Gamma = -D\frac{\Delta c}{\delta} = -k_{22}\frac{\Delta c}{\delta}, \tag{6.2}$$

hence

$$k_{22} = D. \tag{6.3}$$

We can similarly relate k_{11} to the electrical conductance σ using Ohm's Law, which applies to the special case when $\Delta c = 0$.

$$J = \sigma E = -\sigma\frac{\Delta\Phi}{\delta} = -k_{11}\frac{\Delta\Phi}{\delta}, \tag{6.4}$$

hence

$$k_{11} = \sigma. \tag{6.5}$$

Table 6.1 shows the flux of $^{125}I^-$ across the cartilage disk with respect to the applied current density and the potential drop. Using these values we can calculate the four coupling coefficients as follows:

- Since the value of Δc can be considered a constant during the experiment, we can find k_{11} and k_{21} by taking the difference of the current densities and the fluxes respectively.

$$J_1 - J_2 = k_{11}\frac{(\Delta\Phi_2 - \Delta\Phi_1)}{\delta}, \tag{6.6}$$

hence using the measurements of case II and III we find that

$$k_{11} = \delta \cdot \frac{J_1 - J_2}{\Delta\Phi_2 - \Delta\Phi_1} = 370\mu m \cdot \frac{70.8\frac{mA}{cm^2}}{16V} = 1.637 \cdot 10^{-4}\frac{1}{\Omega cm}. \tag{6.7}$$

Furthermore, we know that

$$\Gamma_1 - \Gamma_2 = k_{21}\frac{(\Delta\Phi_1 - \Delta\Phi_2)}{\delta}, \tag{6.8}$$

hence using the measurements of case I and III we find that

$$k_{21} = \delta \cdot \frac{\Gamma_2 - \Gamma_3}{\Delta\Phi_2 - \Delta\Phi_3} = 370\mu m \cdot \frac{-6.148\frac{\%}{hr\,cm^2}}{-16V} = 3.949 \cdot 10^{-6}\frac{\%}{s\,cmV}. \tag{6.9}$$

- Since we now know the value of k_{11} and k_{21}, we can directly find the value of k_{12} and k_{22} using the equation for the current density and the flux and the measurements of case II and III respectively.

$$k_{12} = \frac{\delta \cdot J_2 + k_{11}\Delta\Phi_2}{\Delta c} = \frac{340\mu m \cdot 35.4\frac{mA}{cm^2} - 1.637 \cdot 10^{-4}\frac{1}{\Omega cm}8V}{-1.95\frac{\%}{cm^3}} = 5.436{\cdot}10^{-2}\frac{mA\,cm^2}{\%}, \tag{6.10}$$

and

$$k_{22} = \frac{k_{21}\Delta\Phi_3 - \delta \cdot \Gamma_3}{\Delta c} = \frac{3.949 \cdot 10^{-6}\frac{\%}{s\,cmV}8V - 370\mu m \cdot 6.148\frac{\%}{hr\,cm^2}}{-1.95\frac{\%}{cm^3}} = 1.620{\cdot}10^{-5}\frac{cm^2}{s}. \tag{6.11}$$

From the values of the coupling coefficients we can now calculate the diffusion coefficient and the electrical conductivity of cartilage using equations 6.3 and 6.5.

$$D = k_{22} = 1.620 \cdot 10^{-5}\frac{cm^2}{s}, \tag{6.12}$$

and

$$\sigma = k_{11} = 1.637 \cdot 10^{-4}\frac{1}{\Omega cm}. \tag{6.13}$$

Note that Fick's Law does not directly apply in an open voltage system even if no current density is applied across the tissue. The diffusion of the charged ions can create a Donnan potential at the boundaries, reducing the effective diffusion coefficient. To find the effective diffusion coefficient for open voltage diffusion, we can use Equation 6.1 with $J = 0$.

$$\Gamma = \frac{k_{21}\Delta\Phi - k_{22}\Delta c}{\delta} = -D_{eff}\frac{\Delta c}{\delta}, \tag{6.14}$$

and since $J = 0$ we can also write:

$$0 = -k_{11}\Delta\Phi + k_{12}\Delta c, \tag{6.15}$$

hence:

$$\Gamma = (k_{21}\frac{k_{12}}{k_{11}} - k_{22})\frac{\Delta c}{\delta}, \tag{6.16}$$

giving rise to an effective diffusion coefficient of:

$$D_{eff} = k_{22} - k_{21}\frac{k_{12}}{k_{11}} = 1.620 \cdot 10^{-5}\frac{cm^2}{s} - 3.949 \cdot 10^{-6}\frac{\%}{s\,cm\,V}\frac{5.436 \cdot 10^{-2}\frac{mA\,cm^2}{\%}}{1.637 \cdot 10^{-4}\frac{1}{\Omega cm}}, \tag{6.17}$$

hence

$$D_{eff} = 1.489 \cdot 10^{-5}\frac{cm^2}{s}. \tag{6.18}$$

As we can see, the effective diffusivity of labeled iodide is smaller than the actual value, because the potential drop created by the flux of ions across the tissue exerts a counter force on the solutes. We can similarly calculate an effective conductivity of the tissue and find that the effective conductivity is also smaller than the actual value.

Chapter 7

IGF Transport Through Cartilage

This chapter is dedicated to the insulin-like growth factor transport experiments. We present and describe the experiments in chronological order, discuss the results of each one, and analyze the changes made to the protocol for the following experiment.

7.1 Experiment 1.

The previous IGF-II transport kinetic experiment done by Bhakta [34] (Section 4.4) showed some peculiar results. It was unknown at the time whether these results characterized some unaccounted for phenomena or whether they were a result of experimental artifacts. Therefore, the goal was to repeat these experiments and analyze the results.

7.1.1 Methods

For the transport kinetic study *human recombinant (3-[^{125}I]iodotyrosyl) insulin-like growth factor-2* from Amersham Pharmacia Biotech was used. The lyophilized peptides were reconstituted using $300\mu l$ of 0.01M Acetic Acid and 0.1% BSA. A $5\mu l$ aliquot of the labeled IGF-II was first analyzed for its activity level and found that the sample had $2.286 \cdot 10^4 \frac{cpm}{\mu l}$. For the experiment we used $250\mu l$ of IGF-II, which had a total activity of $5.715 \cdot 10^6 cpm$, and should correspond to $2.1 pmoles$ of IGF-II. Since the purity of the material had been found unacceptable on previous accounts, a standard cleaning procedure was used to establish the desired purity.

The first step of purification of the reconstituted labeled IGF-II was to run it through a $30cm$ by $0.6cm$ Sephadex-G50 column at a flow rate of $1.8\frac{ml}{h}$. We collected 100 fractions

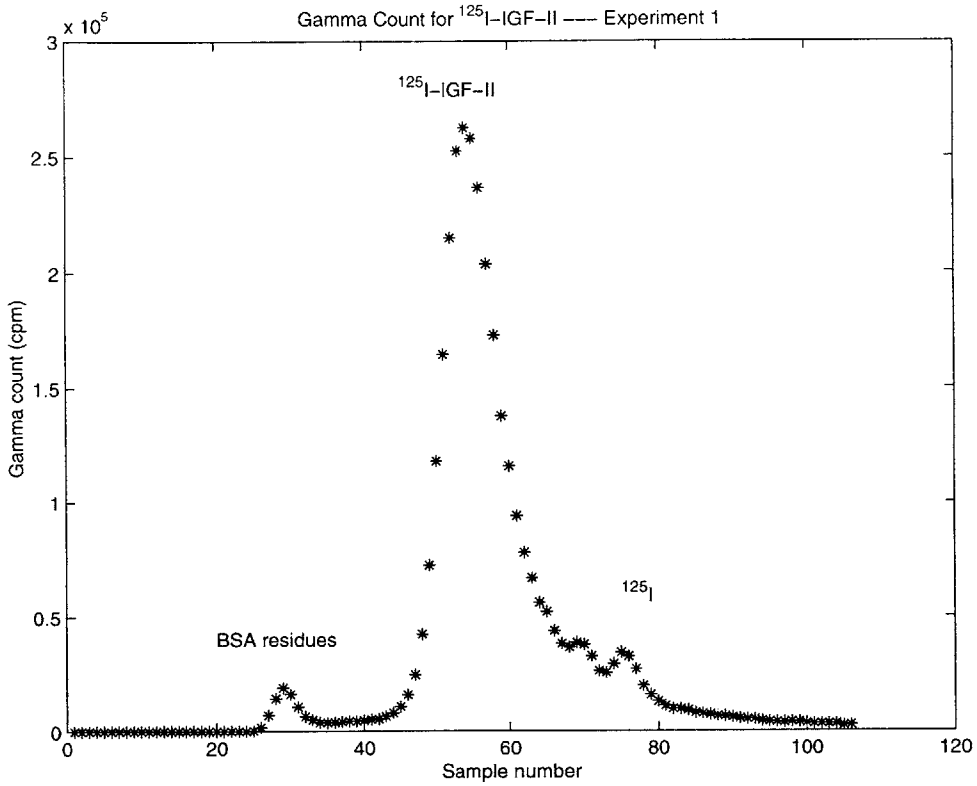

Figure 7-1: Downstream radioactivity for ^{125}I-IGF-II before cleaning. The first peak around sample 30 contains the labeled large aggregates, the second peak around sample 60 has the labeled IGF-II, and the third peak around fraction 75 includes the dissociated free labels.

of $0.3ml$ each to separate the free labels and the large aggregates from the sample. In Figure 7-1, the activity of the fractions are plotted versus the order of the fractions. The first peak around fraction 30 corresponds to large aggregates of BSA residues, radioactive iodide, and labeled IGF-II. The second, much larger, peak around fraction 55 corresponds to labeled IGF-II, and the third smaller peak around fraction 75 contains the free label and/or small fragments containing ^{125}I label. The areas under each peak indicate that the labeled iodide content of the sample was approximately 8%, and the aggregate concentration was even lower. For this experiment, we collected fractions 48 through 65, which contained the labeled IGF-II, and further purified and concentrated the peptides using a centricon-3 filter (with a nominal $3,000MW$ cut-off). This process removed any remaining free label and allowed the exchange of the buffer.

The chamber setup was similar to the one used in the free labeled iodide experiment. The only changes made to the system were the removal of the salt bridge electrodes and the use of three $340\mu m$ thick cartilage disks of $3mm$ radii instead of a single disk.

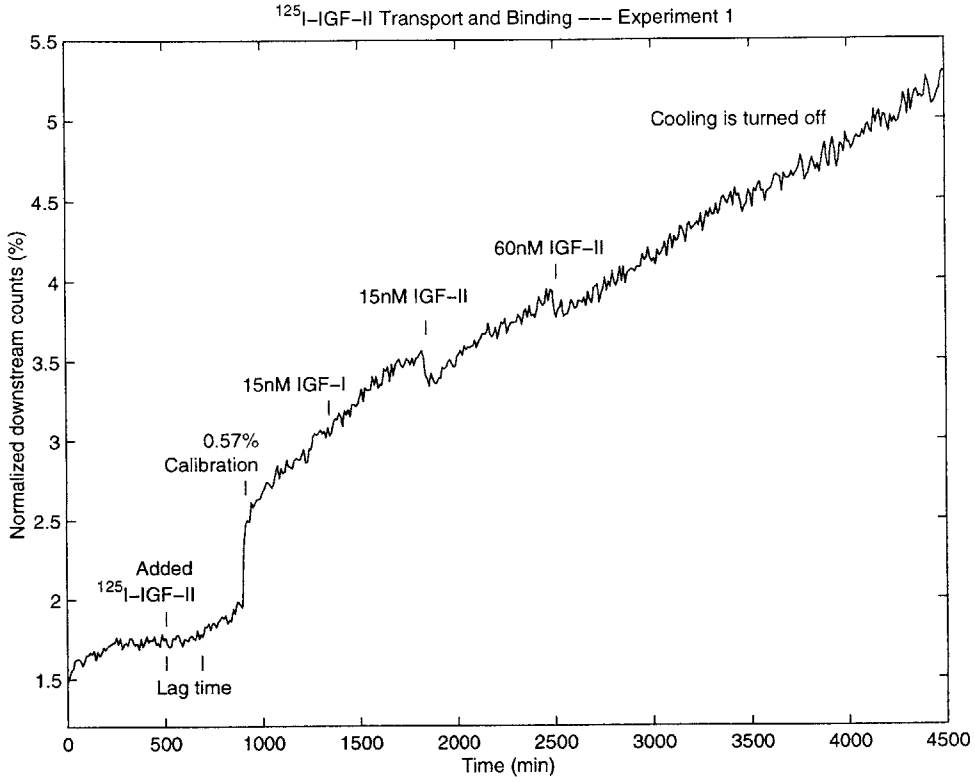

Figure 7-2: The plot shows the ^{125}I-IGF-II downstream radioactivity versus time for Experiment 1, which describes the transport and binding kinetics of the growth factor in cartilage.

The protocol was also similar to that of the free labeled iodide experiment. After a bath equilibration period (0-493min), we added the concentrated ^{125}I-IGF-II to the upstream bath and waited until a constant steady-state flux across the cartilage was established (Figure 7-2). At 902min, the downstream gamma counts were calibrated using $200\mu l$ or 0.57% of the upstream bath. We added 15nM of unlabeled IGF-I at 1331 minutes, 15nM of unlabeled IGF-II at 1827 minutes, and finally 60nM of unlabeled IGF-II at 2499 minutes, to quantify the kinetics of competitive binding of IGF-II to cartilage through hindered transport.

7.1.2 Results

The normalized downstream concentration of IGF-II is shown in Figure 7-2. As the time scale of the experiment indicates, the experiment lasted 75 hours due to the low diffusion rate of radioactive IGF-II. Since the radioactivity of the labeled IGF-II was lower than that of the labeled iodide in the previous experiment, the background noise was quite noticeable.

The two chambers were allowed to equilibrate for several hours. After the radioactivity on the downstream side had stabilized at a constant value, we added the labeled IGF-II to the upstream chamber. The downstream radioactivity established a steady-state linear profile after a lag time of a 180 minutes.

From the linear portion of the graph right after calibration, we could measure the steady-state flux of ^{125}I-IGF-II across the chambers: $2.17 \cdot 10^{-5} \frac{\%}{cm^2 s}$. By the end of the 75 hours, however, the flux had tapered down to $1.47 \cdot 10^{-5} \frac{\%}{cm^2 s}$. It is not yet established why that flux decreased by 30%. It is hypothesized that the decrease in the upstream concentration, binding of the growth factor to the experimental apparatus, and stirring might all play a role in this anomaly.

The dissociation of the $^{125}I^-$ label from the IGF-II was measured using the chromatographic analysis of a $300\mu l$ sample at 3026 minutes from the upstream bath: a 30cm Sephadex G-50 column was used with a flow rate of $1.8 \frac{ml}{hour}$, collecting 100 fractions of $0.3ml$ each as before. The fractions were then analyzed by a gamma counter. Figure 7-3 shows the activity of the fractions collected from the column. Similarly to the previous chromatography done during the purification process, the first peak around fraction 30 corresponds to labeled BSA aggregates, the second peak around fraction 55 corresponds to labeled IGF-II, and the third peak around fraction 75 corresponds to free label. As the areas under the peaks demonstrate, the free label accounted for 20% of the total activity. This indicates a considerable dissociation of ^{125}I-IGF-II to free label and unlabeled IGF-II.

7.1.3 Discussion

As the chromatography of the labeled IGF-II indicated (Figure 7-1), the free labeled iodide content of the peptide was only approximately 8%. The concentration of the larger aggregates was even lower. This prompted the question of whether the cleaning procedure was necessary. Although we continued to clean the IGF-II in the next experiment, we decided to eliminate the cleaning for later experiments if the quality of the labeled IGF-II proved to be adequate.

The greatest problem was the high percentage of dissociated labeled iodide at the end of the experiments. It was hypothesized that the high level of dissociation can be attributed to inefficient cooling; hence, the next experiment was set up inside a refrigerator at $9°C$.

As Figure 7-2 shows, there was a drop in the count after the addition of unlabeled IGF-II

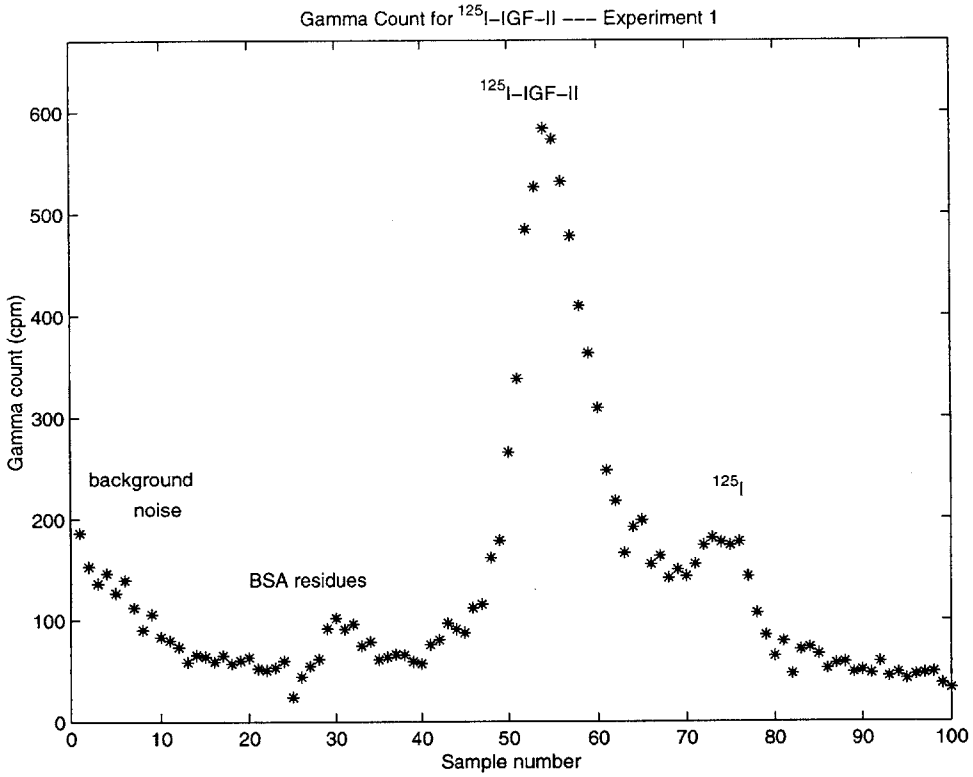

Figure 7-3: Chromatography of an upstream sample taken 3100 minutes into the first IGF-II transport kinetic experiment. The first peak around fraction 30 corresponds to BSA aggregates with ^{125}I or labeled IGF-II, the second peak around fraction 55 corresponds to labeled IGF-II, and the third peak around fraction 75 corresponds to free labels. As the area under the curve indicates, the free iodide content of the upstream bath was significant (approx. 20%) at the end of the experiment.

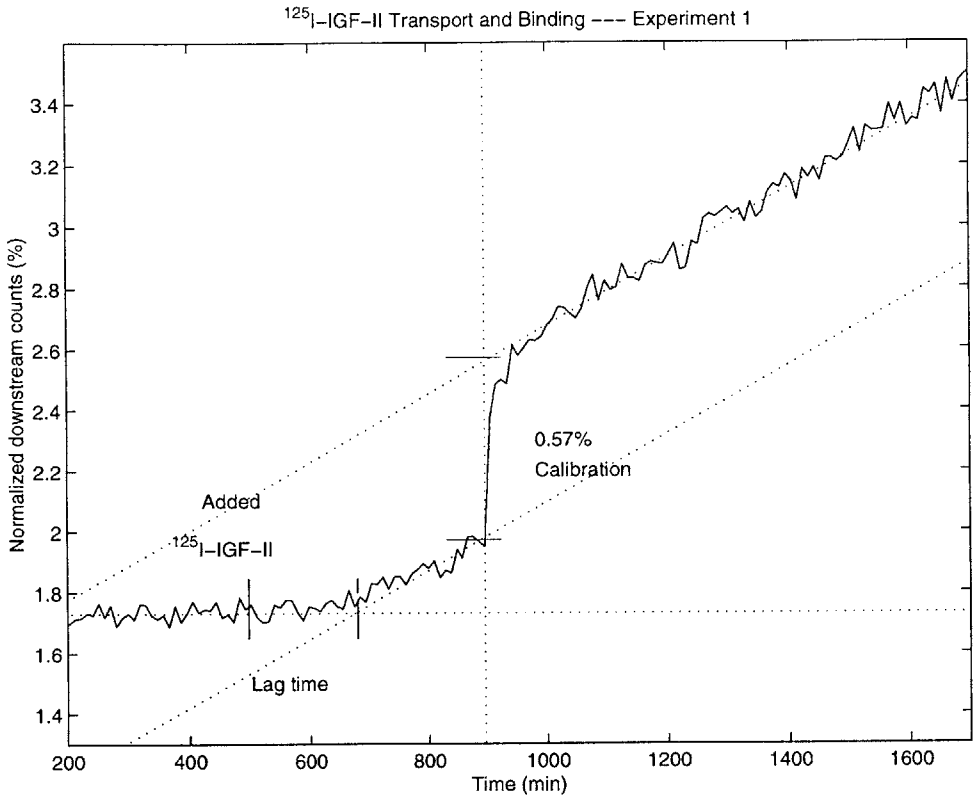

Figure 7-4: The lag time (τ_{lag}) corresponds to the time it takes the growth factor to diffuse across the cartilage disk. The binding of the growth factor to the cartilage further increases the lag time.

to both baths. This was also observed in Bhakta's transport kinetic experiments [34]. After some consideration, we realized that this drop was due to an experimental artifact. It is standard procedure to add a new substance first to the bath with low radioactivity, then to the high activity bath, hence requiring a single pipette tip. In our situation, however, the concentration of unlabeled IGF-II was orders of magnitude greater than that of the labeled IGF-II, thus even an approximately $30s$ delay created a considerable backward flux. Since the stirring of the chambers requires time and it is close to impossible to guarantee that the timing of the addition of unlabeled IGF-II will be simultaneous, we only added the unlabeled IGF-II to the upstream bath in future experiments.

The effective diffusion coefficient of IGF-II could be estimated from the lag time observed after adding the IGF-II to the upstream bath. Using the magnified portion of Figure 7-2 seen in Figure 7-4, the lag time was found to be 180 minutes. From section 3.1.3 we know that:

$$\tau_{lag} = \frac{\delta^2}{6D_{eff}}, \tag{7.1}$$

therefore,

$$D_{eff} = \frac{\delta^2}{6\tau_{lag}} = \frac{(340\mu m)^2}{6 \cdot 180min} \frac{1min}{60s} = 1.78 \cdot 10^{-8} \frac{cm^2}{s}. \tag{7.2}$$

This estimation of D_{eff}, however, is not the diffusion coefficient of IGF-II, but an effective diffusion coefficient that is considerably less due to binding. It is, therefore, expected that the actual diffusion coefficient calculated from the measured flux of the growth factor will be greater than the coefficient found from the lag time.

The diffusion coefficient found by using the Stokes-Einstein Relation in Section 3 was found to be an order of magnitude greater. This is mostly due to the binding of the growth factor to the tissue during transport. The time lag for IGF-II found in my experiments also corresponded well with the lag time measured for IGF-I in the experiments done by Garcia et al. [33]

The diffusion coefficient of radiolabeled materials through the cartilage disk can be found assuming that the potential drop across the cartilage is negligible. The diffusion coefficient in this case is simply the ratio of the change in downstream activity and the upstream concentration:

$$D = -\frac{\Gamma}{\nabla c} \approx \Gamma \frac{\delta}{c^u} = 2.17 \cdot 10^{-5} \frac{\%}{cm^2 s} \frac{340\mu m}{2.77 \frac{\%}{ml}} = 2.66 \cdot 10^{-7} \frac{cm^2}{s}. \tag{7.3}$$

The diffusion coefficient calculated this way, however, gives us the combined diffusion of the labeled IGF-II and the free labeled iodide. Since in our results we found that the dissociation after 3100 minutes is already significant (20%), and we know that the diffusion coefficient of a small iodide will be much greater than the diffusion coefficient of IGF-II, we must account for the free label flux in order to find the IGF-II diffusion coefficient and the number of binding sites within the tissue.

Assuming that at time t=0 we did not have any free label, and at time t=3100min we had 20% of the labels dissociated from the IGF-II, we can calculate the time constant of dissociation assuming an exponential dissociation function:

$$\tau = -\frac{3100min}{ln(1 - 0.2)} = 1.389 \cdot 10^4 min. \tag{7.4}$$

If we are trying to find the diffusion coefficient of IGF-II, it is enough to look at the linear

portion of our graph after calibration between 902 and 1827 minutes. The governing equations during this portion, assuming that only $^{125}I^-$ and ^{125}I-IGF-II contribute significantly to the total radioactive flux, are the following:

$$\Gamma_{2*} = \Gamma_* - \Gamma_I \tag{7.5}$$

where Γ_{2*} is the labeled IGF-II flux, Γ_* is the total radioactive flux, and Γ_I is the labeled iodide flux.

Using the definition of flux we know that

$$\Gamma_* = \frac{1}{A}\frac{\Delta N}{\Delta t} \tag{7.6}$$

since the flux is constant according to our results. Using Fick's First Law, we also know that

$$\Gamma_I = D_I\frac{c_I^u - c_I^d}{\delta} \approx D_I\frac{c_I^u}{\delta} = D_I\frac{c_{2*}^\circ}{\delta}(1 - e^{-t/\tau}) \tag{7.7}$$

and

$$\Gamma_{2*} = D_2\frac{c_{2*}^\circ e^{-t/\tau}}{\delta} \tag{7.8}$$

assuming that the diffusion of ^{125}I-IGF-II is steady and the downstream concentration of ^{125}I-IGF-II is negligible.

Combining the above equations we can find the diffusion coefficient of IGF-II has a negative value, which is impossible. Hence, our assumptions are not valid! Some of the assumptions such as the downstream concentration of $^{125}I^-$ being negligible, and the calculated value of τ being accurate, are incorrect. Since our results for D_2 are very sensitive to τ, an inaccurate value can easily give a nonsensical value for D. The solution to this problem is to prevent the dissociation of labeled IGF-II by cooling down its environment.

7.2 Experiment 2.

The second IGF-II transport kinetic experiment was based on the first one with a few alterations. Even though this experiment still had some complications, the results were noteworthy, and quantitative calculations could be carried out based on the results.

7.2.1 Method

The experimental procedures remained the same as for Experiment 1, except for a few minor changes:

1. Unlabeled growth factors were added only to the upstream chamber. This prevented uncontrollable backwards flux due to inevitable delays between the equilibration of the two chambers.

2. Instead of using a circulating cooling system, the chamber setup was moved to a refrigerator at $9°C$ for the length of the experiment. This was necessary to maintain the integrity of the labeled IGF-II and reduce the dissociation of the labels from the growth factor.

3. No IGF-I was added during the experiment since according to both Experiment 1 and the experiments done by Bhakta (Section 4.4), IGF-I has no effect on the transport kinetics of IGF-II across the cartilage.

4. I tested the case of adding 0.1nM unlabeled IGF-II to see whether competition for binding sites occurred at lower concentrations. 0.1nM was chosen also because it is on the same order of magnitude as the labeled IGF-II concentration of the upstream bath.

5. The calibration was done after the experiment had finished running to minimize the amount of radioactive material that was found in the downstream chamber at the end of the run.

6. The thickness of the disks was $330\mu m$ instead of $340\mu m$.

7. I also added more proteinase inhibitors to ensure that minimal tissue degradation occurred over the course of the experiment. These inhibitors were $5mM$ benzamidine HCl and $1mM$ PMSF.

7.2.2 Results

The preparatory chromatographic results of the ^{125}I-IGF-II can be seen in Figure 7-5. The result indicate that the labeled IGF-II wad excellent quality, containing less than 2% of labeled iodide and even less large aggregates. We used fractions 47–62 for the experiments.

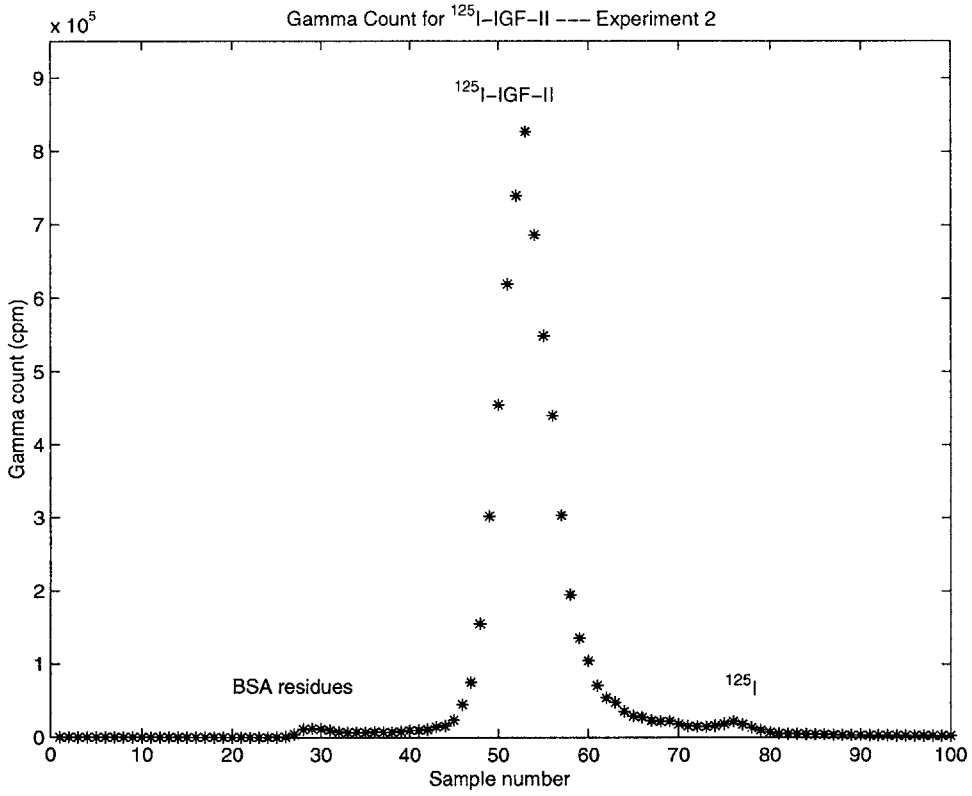

Figure 7-5: Chromatographic analysis of the ^{125}I-IGF-II before cleaning. The major peak around fraction 55 is the labeled growth factor, while the two smaller peaks around fraction 30 and 75 are the large aggregates and the labeled iodide respectively. The results indicate less than 2% labeled iodide, and even less large aggregates.

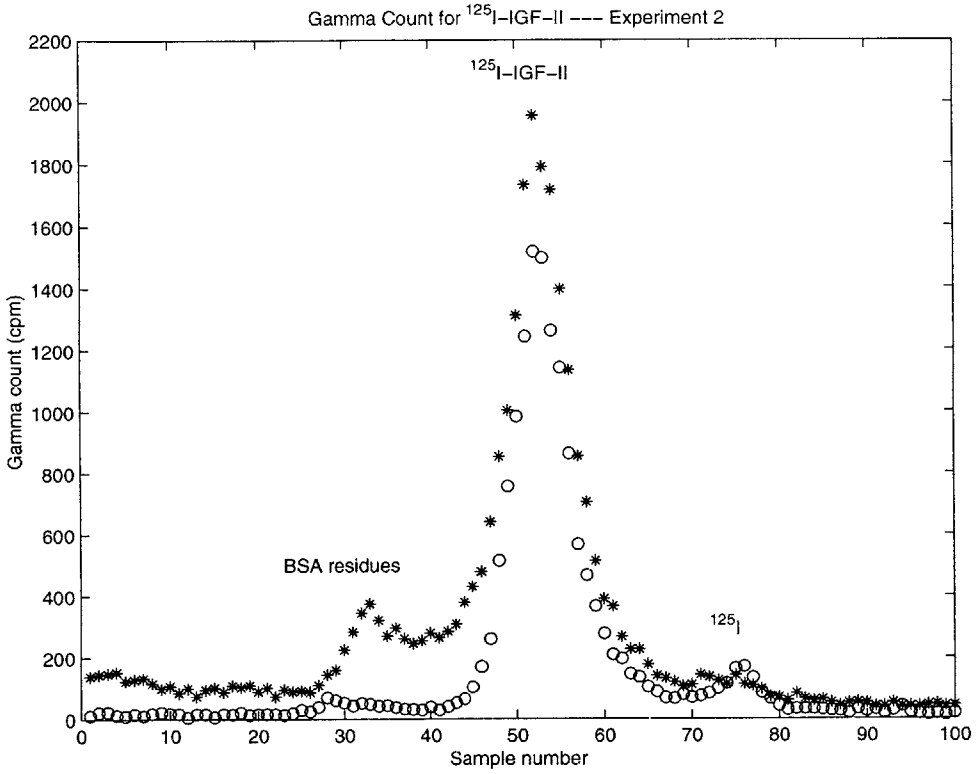

Figure 7-6: Chromatography of upstream samples at the beginning (*) and end (o) of the experiments. Notice the low peak of iodide around fraction 75, and the disappearance of the large aggregates peak around fraction 30.

An upstream sample was also analyzed at the beginning (1175 minutes) and at the end (3875 minutes) of the experiment. The chromatographic analysis of the samples can be seen in Figure 7-6. As the figure indicates, the iodide content of the sample was negligible ($< 8\%$) in both cases indicating minimal dissociation. The more interesting part of the curve is the concentration of large aggregates. In the beginning of the experiment, the concentration of large aggregates was significant (approx. 19 %). At the end of the experiment, however, virtually no contribution could be found in the upstream sample.

The results of the experiment can be seen in Figure 7-7. As the figure indicates, there was a lag time of 185 minutes after the addition of the labeled IGF-II. During steady-state, a constant flux of $7.27 \cdot 10^{-5} \frac{\%}{cm^2 s}$ was established. The addition of $0.1nM$ unlabeled IGF-II did not affect the flux of the labeled IGF-II, but the addition of $15nM$ unlabeled IGF-II had a significant effect on the downstream counts. It can also be seen that the downstream radioactivity curve is "bumpy." These "bumps" were attributed to the occasional failure of stirring due to difficulties with the stirring bars.

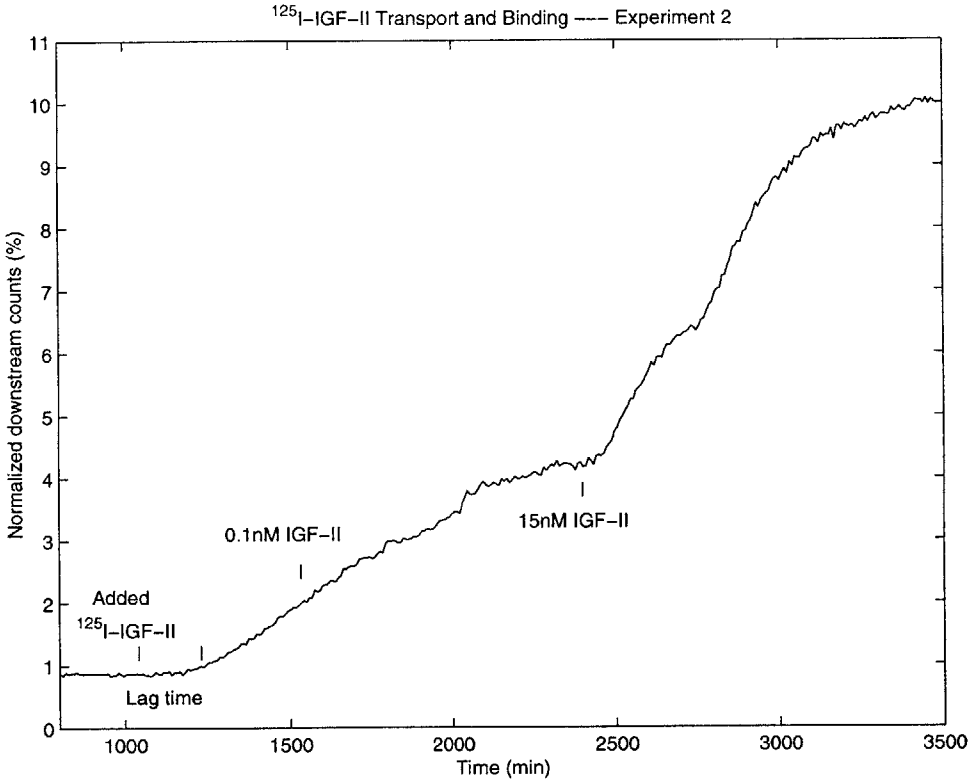

Figure 7-7: The downstream radioactivity of Experiment 2 is plotted versus time. Notice the lag time after the labeled IGF-II has been added, and the transient increase in flux after the addition of 15nM unlabeled IGF-II.

The difference between the expected downstream count at 3500 minutes due to simple flux of the labeled IGF-II and the actual value should have corresponded to the previously cartilage-bound labeled IGF-II that was displaced by the unlabeled IGF-II. This difference was found to be 1.87%.

7.2.3 Discussion

The lag time found in this experiment was 185 minutes, which agrees well with the 180 minutes found in the previous experiment. Using this new lag time to calculate the effective diffusion coefficient we find that

$$D_{eff} = \frac{\delta^2}{6\tau_{lag}} = \frac{(330\mu m)^2}{6 \cdot 185 min} \frac{1 min}{60 s} = 1.64 \cdot 10^{-8} \frac{cm^2}{s}. \tag{7.9}$$

This value is within 8% of the previously found diffusion coefficient.

A steady-state flux of $7.27 \cdot 10^{-5} \frac{\%}{cm^2 s}$ was measured, which is 3.35 times greater than the $2.17 \cdot 10^{-5} \frac{\%}{cm^2 s}$ found in the previous experiment. It is still unclear why the steady-state flux was 3.35 times higher than in the previous experiment. Some of the possibilities are that the stirring might have been more efficient, hence decreasing the stagnant layers on the cartilage disks and increasing flux. Another possibility is that a leak might have been present, but the presence of the lag time makes this possibility rather unlikely.

The "bumps" in the graph can be attributed to the lack of stirring, since the checkups on the system (and the fixing of the stirring bars) corresponded well with the reestablishment of the original slope. The lack of stirring in these situations created a thick stagnant layer of solutions on both sides of the cartilage, forcing the labeled IGF-II to diffuse across this layer as well as the cartilage. Since diffusion is much slower than convection, this resulted in a significant decrease of the labeled IGF-II flux.

The results show that the addition of 0.1nM of unlabeled IGF-II had no noticeable effect on the transport kinetics of labeled IGF-II. On the other hand, we can see that 15nM of unlabeled IGF-II created a significant jump in the downstream count, indicating possible competitive binding to the tissue. These results correlate well with Bhakta et al.'s [19] finding that competition occurs only at concentrations greater than $10nM$.

The lack of stirring before the 15nM unlabeled IGF-II had been added might also explain the surprisingly high jump in the downstream count. If a stagnant layer had been established

on the downstream side with a higher concentration of labeled IGF-II, then when the stirring was continued, the labeled growth factor in this region gradually was mixed into the downstream bath, causing an additional increase in the downstream radioactivity.

7.3 Experiment 3.

7.3.1 Methods

The basic experimental setup remained the same as in Experiment 2 except for:

1. The peptides were reconstituted using 4mM HCl, 1% BSA solution.
2. The cleaning procedure of the labeled IGF-II was replaced by a chromatographic analysis of a fraction of the original sample. In case the purity would have proven inadequate, the rest of the labeled IGF-II would have been cleansed before proceeding. However, since the purity was acceptable, the cleaning procedures were omitted.
3. 15nM IGF-I was used to show, on the same curve, that there is no competition between the two types of growth factors for binding sites within the cartilage.
4. The calibration was done at the beginning of the experiment to gauge the downstream values while the experiment was running.
5. 15nM and 60nM of unlabeled IGF-II were used to test the competition for IGF-II binding sites, since the 0.1nM of unlabeled IGF-II had no effect in the previous experiment.
6. After the standard protocol, salt bridge electrodes were added to the chambers, and $+10mA$ and $-10mA$ total current was applied across the cartilage as a pilot study of the electrophoretic transport kinetics of IGF-II.
7. The disks had an average thickness of $360\mu m$ instead of the previously used $340\mu m$ and $330\mu m$.

7.3.2 Results and Discussion

Figure 7-8 shows the chromatographic analysis of the labeled IGF-II. The analysis showed

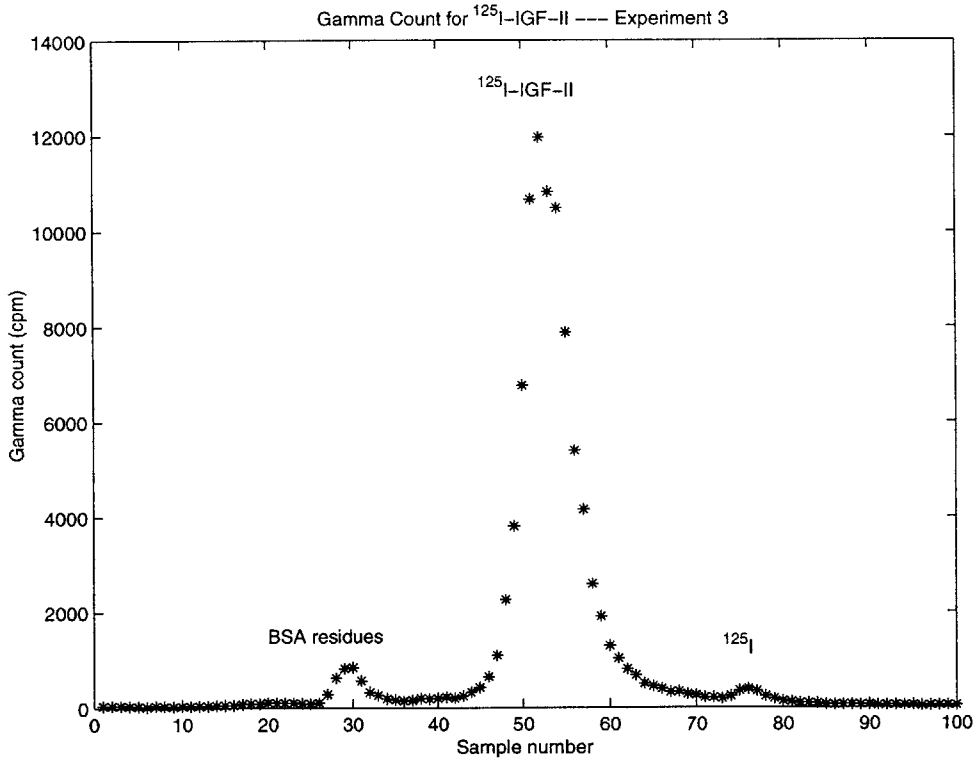

Figure 7-8: Chromatographic analysis of labeled IGF-II. It can be seen that the labeled iodide concentration of the sample is less than 3%, and the large aggregate content is below 5%.

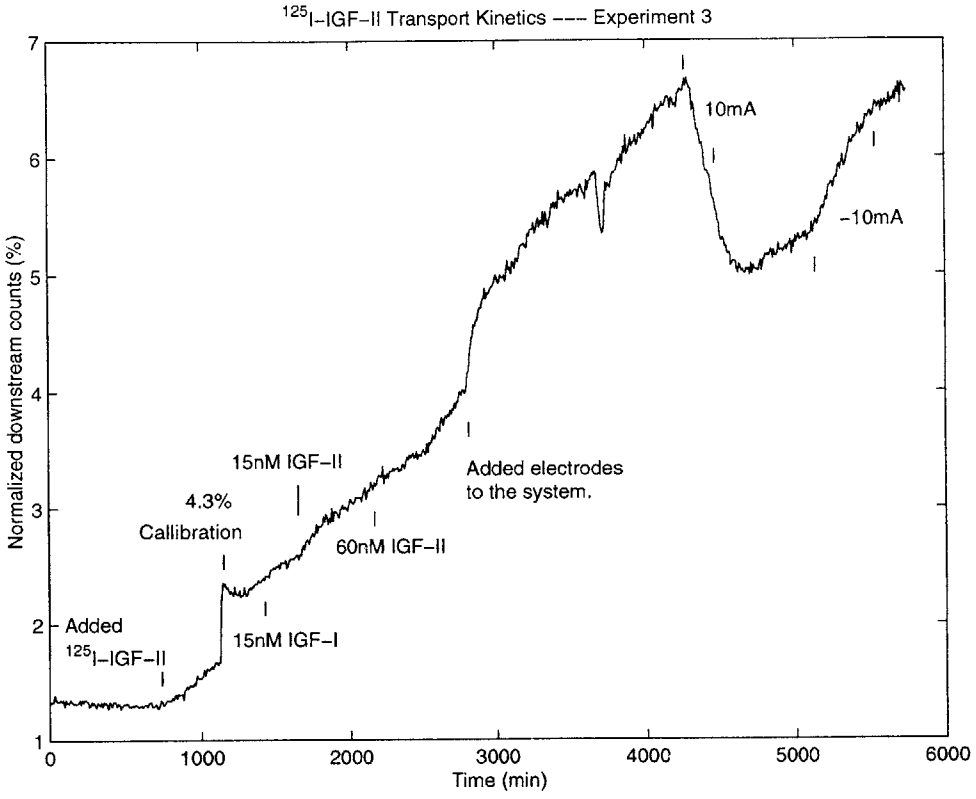

Figure 7-9: The downstream radioactivity of Experiment 3 is plotted versus time.

that the purity of the labeled growth factor was very good, having a labeled iodide concentration of less than 3% and a labeled large aggregate concentration of less than 5%. Based on these results, the cleaning procedures were omitted and the remaining reconstituted peptides were used for the experiment.

Figure 7-9 presents the downstream count versus time. Figure 7-10 is a closeup of the first 500-2800 minutes, which show the competitive binding study of IGF-II.

Surprisingly, a lag time between the addition of the growth factor and the establishment of steady-state was not detected. This may suggest a leak between the two chambers. The magnitude of the flux during steady-state, however, was at the expected value, making a leak unlikely.

During steady-state, the flux was measured to be $1.97 \cdot 10^{-5} \frac{\%}{cm^2 s}$. This is only 91% of the steady-state flux measured in Experiment 1, and only 27% of the steady-state flux measured in Experiment 2. The low flux indicates the lack of a leak, but then the disappearance of the lag time becomes even more puzzling.

A final thing that's worth noting is the slight increase in flux after the addition of 15nM

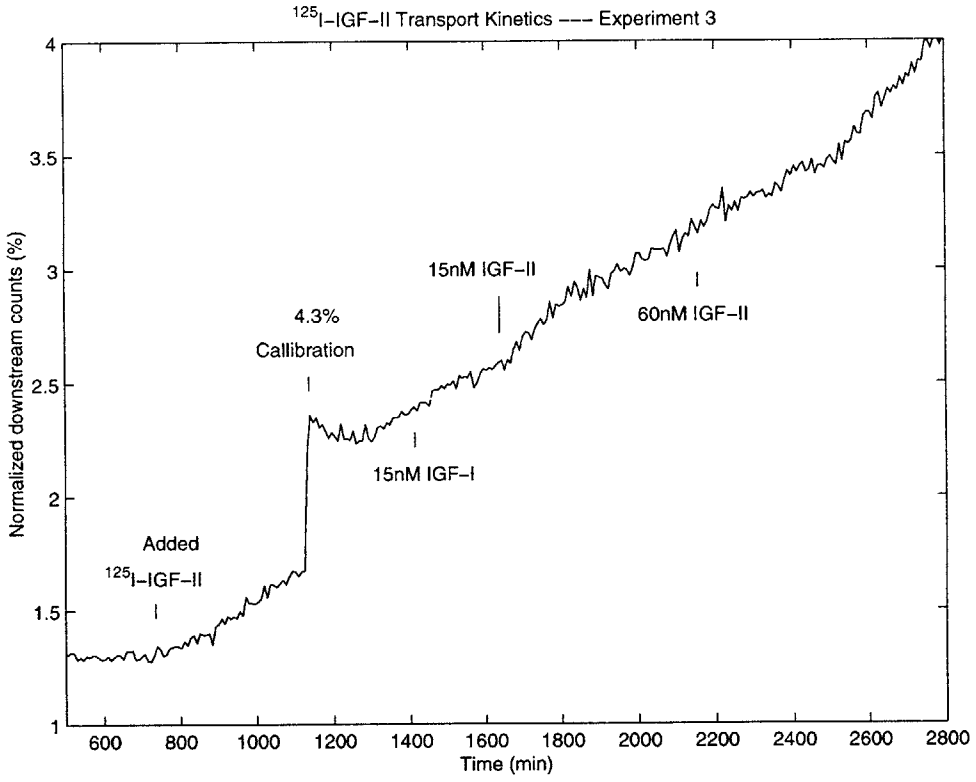

Figure 7-10: A magnified view of the downstream radioactivity of the first half of Experiment 3. This part of the experiment was the standard binding transport kinetic study.

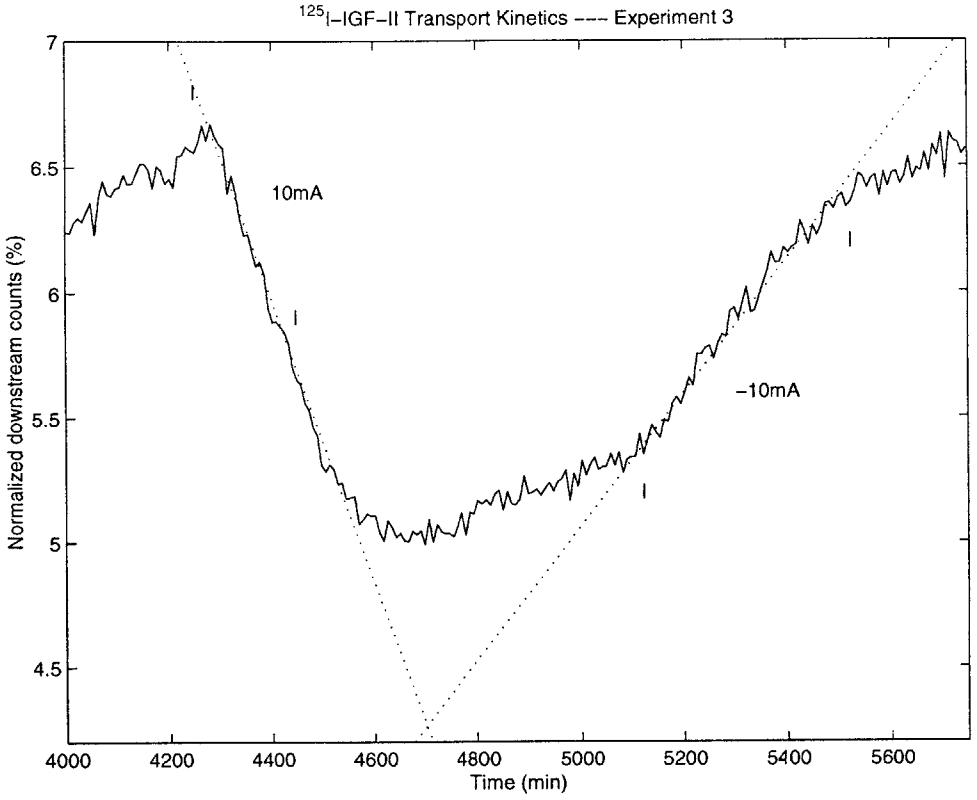

Figure 7-11: A magnified view of the downstream radioactivity for the second half of Experiment 3. This was the pilot study for electrophoretic transport kinetic studies of IGF-II.

IGF-II. An increase was predicted by the competitive binding of unlabeled and labeled IGF-II to the tissue, however, the increase is only minimal, 0.08%, compared to the increase of 1.87% observed in Experiment 2. It is possible that the greater increase seen in the previous experiment was due to the labeled IGF-II found in the stagnant layer, which was mixed into the downstream bath after the addition of unlabeled IGF-II. However, this is only a speculation, and requires further investigation.

Figure 7-11 is a closeup of the pilot electrophoretic study of the insulin like growth factor. As Figure 7-9 indicated, the electrodes were contaminated by free labeled iodide, hence the steady-state flux values during electrophoresis must be considered with the knowledge that free label contributes significantly to the flux. The actual measured values of the flux are summarized in Table 7.1.

Finally, we looked at the chromatographic analysis of the upstream solution to verify that the purity of the solution was adequate. As Figure 7-12 indicates, the free label content of the upstream solution was less than 3%, but high concentrations (21%) of aggregates were

	Current Density, J	Normalized Flux, Γ	Potential Drop, $\Delta\Phi$	Concentration Drop, Δc
I	$0\frac{mA}{cm^2}$	$1.97 \cdot 10^{-5}\frac{\%}{cm^2 s}$	?	$2.77\frac{\%}{cm^3}$
I	$11.8\frac{mA}{cm^2}$	$-1.12 \cdot 10^{-4}\frac{\%}{cm^2 s}$	-7V	$2.69\frac{\%}{cm^3}$
I	$-11.8\frac{mA}{cm^2}$	$5.31 \cdot 10^{-5}\frac{\%}{cm^2 s}$	8V	$2.69\frac{\%}{cm^3}$

Table 7.1: Steady-state values for the relevant electrophoretic variables during the pilot study.

again detected.

At the end of the experiment, the upstream solution was found to be significantly contaminated as Figure 7-13 indicates. The free labeled iodide content of the upstream solution was found to be around 20%, and the aggregates dominated 25% of the upstream activity. Therefore, the values found in the electrophoretic pilot studies must only be taken qualitatively, not quantitatively.

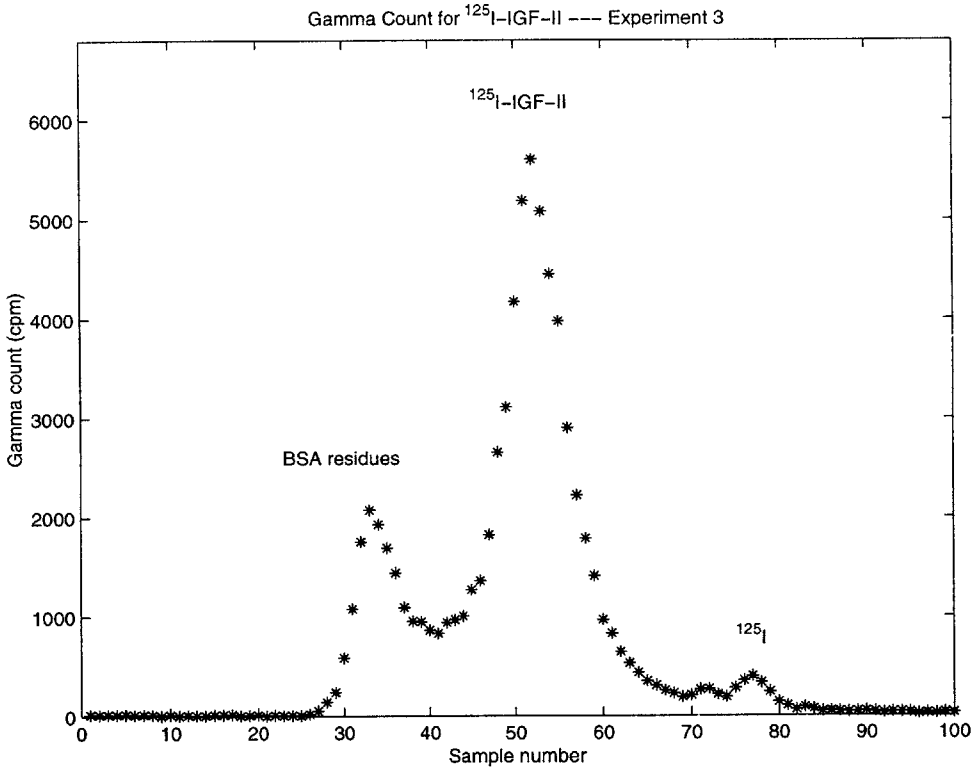

Figure 7-12: Chromatographic results of an upstream sample taken after the addition of the labeled growth factor to the upstream bath in Experiment 3.

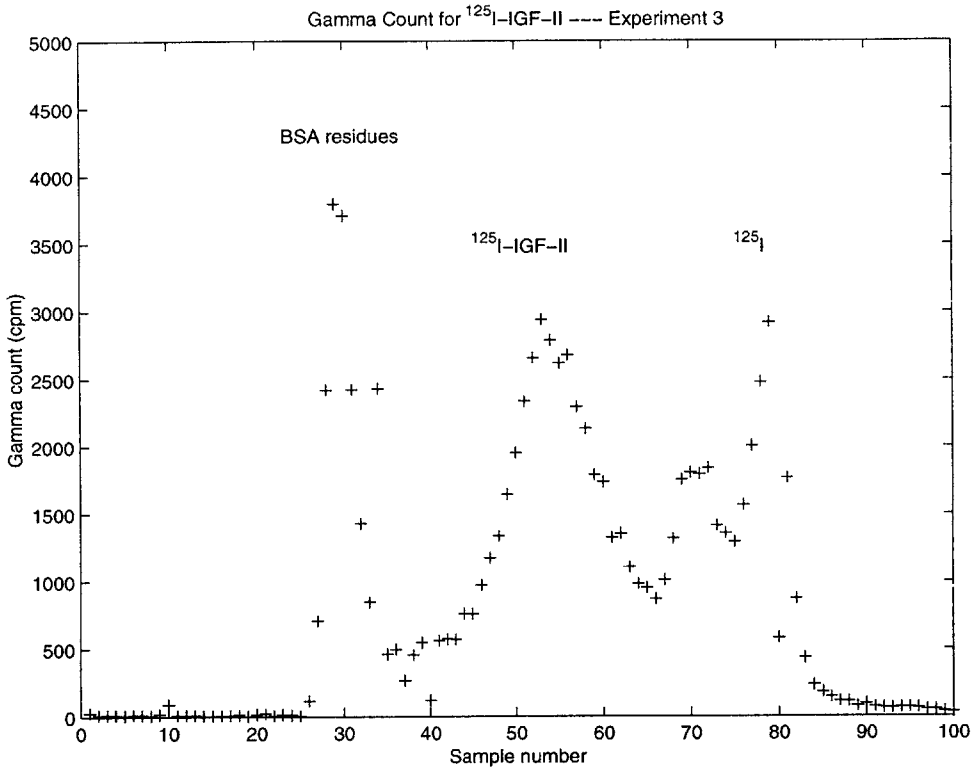

Figure 7-13: Chromatographic results of an upstream sample taken at the end of Experiment 3.

Chapter 8

Conclusions

8.1 Summary

Articular cartilage provides cushioning and distributes load over articulating joint surfaces. Healthy cartilage is extremely resilient to shear and compressive stress, but its homeostasis is easily disrupted due to its low cell count and perfusion rate. The transport of macromolecules, therefore, plays a rate limiting role in tissue regeneration after injury. The goal of this thesis was to study the transport of IGF-II, a regulatory solute, in the tissue.

In this study we have shown that even though the size of IGF-II is on the order of the average intermolecular spacing within the tissue, transport and binding do occur. We have successfully found the characteristic time scale of IGF-II transport and binding. Furthermore, we have presented proof of the reversible nature of IGF-II binding and showed that at physiological concentrations IGF-I is not capable of competing with IGF-II for binding sites.

8.2 Future Work

The work that is described in this thesis in only the beginning of a whole series of transport kinetic experiments. In order to fully describe the behavior of macromolecular transport and binding within cartilage, the following experiments will be performed in the near future:

- Testing the stirring apparatus of the current setup. This can be done by testing labeled iodide transport across tissue in the absence and presence of stirring.

- Testing the competition between IGF-II with IGF-I for binding sites by running the transport kinetic studies using labeled IGF-I, and adding graded amounts of IGF-II to the upstream bath.
- Testing the effect of an applied electric field on the transport of IGF-I and IGF-II.
- Measuring the open-circuit voltage during future transport experiments.
- Testing the effect of tissue degradation and altered tissue charge on transport by using degrading enzymes or altering the pH.

The above experiments should provide sufficient information to quantify the transport kinetic and binding properties of IGF-I and IGF-II, and hence complete this study.

Bibliography

[1] B. Y. Lin. Characterization of the properties of cartilage in the hartley guinea pig spontaneous osteoarthritis model. Master's project, Massachusetts Institute of Technology, Electrical Engineering and Computer Science Department, June 1997.

[2] J. J. Zhu. Transport studies of chondroitin sulfate disaccharide through articular cartilage. Master's project, Massachusetts Institute of Technology, Electrical Engineering and Computer Science Department, June 1997.

[3] A. Maroudas. *Physical Chemistry of Articular Cartilage and the Intervertebral Disc. In Joints and Synovial Fluid, pp. 239-291. (ed. L. Sokoloff)*, volume 2. Academic Press, New York, 1980.

[4] R. A. Stockwell and G. Meachim. *The Chondrocytes.* Grune & Stratton, New York, NY, 1972.

[5] A. M. Garcia. *Mechanisms of Macromolecular Transport Through Articular Cartilage: Relevance to Loading.* PhD dissertation, Massachusetts Institute of Technology, Department of Harvard-M.I.T. Division of Health Sciences and Technology, June 1996.

[6] T. M. Quinn, A. A. Maung, A. J. Grodzinsky, E. B. Hunziker, and J. K. Sandy. Physical and biological regulation of proteoglycan turnover around chondrocytes in cartilage explants: Implications for tissue degradation and repair. unpulished document, 1999.

[7] T. I. Morales. Transforming growth factor-β and insulin-like growth factor-1 restore proteoglycan metabolism of bovine articular cartilage after depletion by retinoic acid. *Archives of Biochemistry and Biophysics*, 315(1):001–009, Nov. 1994.

[8] H. Muir. The chondrocyte, architect of cartilage. *BioEssays*, 17(12):1039–1048, 1995.

[9] W. K. Manning and W. M. Bonner. Isolation and culture of chondrocytes from human adult articular cartilage. *Arthritis Rheum.*, 10(235), 1967.

[10] A. L. Lehninger, D. L. Nelson, and M. M. Cox. *Principles of Biochemistry.* Worth Publishers, New York, NY, second edition, 1993.

[11] J. F. Bateman, S. R. Lamande, and J. A. M. Ramshaw. *Collagen Superfamily in Extracellular Matrix*, volume 2. Overseas Publishers Association, Amsterdam, The Netherlands, first edition, 1996.

[12] D. R. Eyre, A. Apon, J.-J. Wu, L. H. Ericsson, and K. A. Walsh. Collagen type ix: evidence for covalent linkages to type ii collagen in cartilage. *Federation of European Biochemical Societies Letters*, 220(2):337–341, June 1987.

[13] R. N. Wight, D. K. Heinegard, and V. C. Hascall. *Cell Biology of Extracellular Matrix.* Plenum Press, New York, NY, second edition, 1991.

[14] D. Heinegard and A. Oldberg. Structure and biology of cartilage and bone matrix noncollagenous macromolecules. *FASEB J.*, 3:2042–2051, 1989.

[15] R. Schneiderman, E. Snir, O. Popper, J. Hiss, H. Stein, and A. Maroudas. Insulin-like growth factor-1 and its complexes in normal human articular caritlage: Studies of partition and diffusion. *Archives of Biochemistry and Biophysics*, 324(1):159–172, Dec. 1995.

[16] T. L. Blundell, S. Bedarkar, and R. E. Hunbel. Tertiary structures, receptor binding, and antigenicity of insulin-like growth factors. *Federation Proc.*, 42:2592–2597, 1983.

[17] R. Schneiderman, N. Rosenberg, J. Hiss, P. Lee, F. Liu, R. L. Hintz, and A. Maroudas. Concentration and size distribution of insulin-like growth factor-1 in human normal and osteoarthritic synovial fluid and cartilage. *Archives of Biochemistry and Biophysics*, 324(1):173–188, Dec. 1995.

[18] T. I. Morales. The role and content of endogenous insulin-like growth factor-binding proteins in bovine articular cartilage. *Archives of Biochemistry and Biophysics*, 343(2):164–172, July 1997.

[19] N. R. Bhakta, T. I. Morales, E. H. Frank, and A. J. Grodzinsky. Insulin-like growth factor (igf) bind specifically to endogenous igf binding proteins in adult articular cartilage. ORS abtract, Feb. 1999.

[20] A. Fick. On liquid diffusion. *Philos. Mag.*, 10:30-39, 1855.

[21] T. F. Weiss. *Cellular Biophysics*, volume 2. MIT Press, Cambridge, MA, first edition, 1996.

[22] A. Einstein. *Investigations on the Theory of the Brownian Movement, R. Furthe and A. D. Cowper, eds.* Dover, New York, NY, 1956.

[23] W. M. Deen. *Analysis of Transport Phenomena.* Oxford University Press, New York, NY, first edition, 1998.

[24] G. G. Stokes. On the effect of the internal friction of fluids on the motion of pendulums. *Trans. Camb. Phil. Soc.*, 9:6–106, 1851.

[25] A. J. Grodzinsky. Fields, forces and flows in biological tissues and membranes. Course notes for 6.561J at MIT, 1998.

[26] I. Binderman, D. Somjen, Z. Shimshoni, J. Levy, H. Fischler, and R. Korenstein. Stimulation of skeletal-derived cell cultures by different electric field intensities is cell-specific. *Biochim Biophys Acta*, 844:273–279, 1985.

[27] J. P. Elliott, R. L. Smith, and C. A. Block. Time-varying magnetic fields; effects of orientiation on chondrocyte proliferation. *Journal of Orthopaedic Research*, 6:259–264, 1988.

[28] R. L.-Y. Sah, Y.-J. Kim, J.-Y. Doong, A. J. Grodzinsky, A. H. K. Plaas, and J. D. Sandy. Biosynthetic response of cartilage explants to dynamic compression. *Journal of Orthopaedic Research*, 7:619–636, 1989.

[29] A. J. Grodzinsky, Y.-J. Kim, M. D. Buschmann, A. M. Garcia, T. M. Quinn, and E. B. Hunziker. Response of the chondrocyte to mechanical stimuli. Osteoarthritis. Ed: Brandt, Doherty, Lohmander.

[30] L. Lippiello, D. Chakkalakal, and J. F. Connolly. Pulsing direct current-induced repair of articular cartilage in rabbit osteochondral defects. *Journal of Orthopaedic Research*, 8:266–275, 1990.

[31] H. Liu, J. Abbott, and J. A. Bee. Pulsed electromagnetic fields influence hyaline cartilage extracellular matrix composition without affecting molecular structure. *Osteoarthritis and Cartilage*, 4:63–76, 1996.

[32] L. A. MacGinitie, Y. A. Gluzband, and A. J. Grodzinsky. Electrical field stimulation can increase protein synthesis in articular cartilage explants. *Journal of Orthopaedic Research*, 12:151–160, 1994.

[33] A. M. Garcia, E. H. Frank, S. B. Trippel, and A. J. Grodzinsky. Igf-1 transport in cartilage: Effects of binding and intratissue fluid flow. ORS abtract, Feb. 1997.

[34] N. R. Bhakta. Transport kinetics of insulin-like growth factor-2. unpublished data, 1997.

[35] I. N. Levine. *Physical Chemistry.* McGraw-Hill Book Company, New York, NY, third edition, 1988.